J. Fluid Mech. (1973), *vol.* 59, *part* 2, *pp.* 337–368
Printed in Great Britain

Upwelling of a stratified fluid in a rotating annulus: steady state. Part 2. Numerical solutions

By J. S. ALLEN
Department of Aerospace Engineering, The Pennsylvania State University

(Received 29 June 1972)

Numerical solutions of finite-difference approximations to the Navier–Stokes equations have been obtained for the axisymmetric motion of a Boussinesq liquid in a rigidly bounded rotating annulus. For most of the cases studied, a temperature difference is maintained between the top and bottom surfaces such that essentially a basic stable density stratification is imposed on the fluid. The side walls are thermally insulated and the motion is driven by a differential rotation of the top surface. Approximate steady-state solutions are obtained for various values of the Rossby number ϵ and the stratification parameter $S = N^2/\Omega^2$, where N is the Brunt–Väisälä frequency and Ω is the rotational frequency. The changes in the flow field with the variation of these parameters is studied. Particular attention is given to an investigation of the meridional, or upwelling, circulation and its dependence on the stratification parameter. The effects on the flow of different boundary conditions, such as an applied stress driving, specified temperature at the side walls and an applied heat flux at the top and bottom surfaces, are also investigated.

1. Introduction

A linear theory for the effect of a stable density stratification on the steady motion of a contained rotating fluid has been developed by Barcilon & Pedlosky (1967*a*, *b*). The time-dependent behaviour of contained rotating stratified fluids has also been studied by several authors (see, for example, Siegmann 1971 for references), primarily through an examination of linear-theory solutions to the initial-value spin-up problem.

In view of the interesting flow phenomena that are predicted in these studies and of the close relationship of the results to geophysical problems, it appears that an investigation of the properties of flows in rotating stratified fluids, under conditions where nonlinear effects can be important, would be especially appropriate at this time. The use of numerical solutions of finite-difference approximations to the full governing equations presents a convenient method for this type of study and that is the approach we have taken here.

The problem investigated is the axisymmetric laminar motion of a Boussinesq liquid in a rigidly bounded rotating annulus. The axis of the annulus is aligned with the (vertical) rotation vector, which is anti-parallel to the gravity vector. A temperature difference is maintained between the horizontal top and bottom surfaces of the annulus such that essentially a basic stable density stratification

is imposed on the fluid. For most of the cases investigated, the (vertical) cylindrical side walls are thermally insulated and the fluid motion is driven mechanically by a differential rotation of the top surface. Numerical solutions are obtained for the transient response of the fluid, initially in a state of static equilibrium, to an impulsively applied differential, rigid rotation of the top surface. Time-dependent solutions are calculated by finite-difference approximations to the unsteady equations until the flow becomes approximately steady (see §5). These approximate steady-state solutions are the ones that are presented here. The nature of the transient adjustment of the fluid is also of considerable interest. That naturally forms a somewhat separate study, however, and is not included here.

Solutions are obtained for various values of the stratification parameter $S = N^2/\Omega^2$, where N is the Brunt–Väisälä frequency and Ω is the rotational frequency. The effects of nonlinearities are investigated by varying the Rossby number. Most of the solutions are obtained with the top surface rotating in a sense which is opposite to that of the basic rotation. In that case there is an upwelling of fluid at the outer side wall of the annulus. Particular attention is given to a study of the meridional, or upwelling, circulation and its dependence on the stratification parameter.

The effects on the flow of different boundary conditions are also investigated. These are (i) a rotation of the top surface in the same sense as the basic rotation, in which case there is a downwelling of the fluid at the outer side wall, (ii) an applied stress, rather than an applied velocity, driving, (iii) an applied heat flux, rather than a fixed temperature, at the top and bottom surfaces, and (iv) a specified temperature, rather than zero heat flux, at the side walls.

Linear-theory solutions for the steady motion in an annulus with the stratification parameter S in a range such that $\bar{S} = \frac{1}{4}\sigma S \geqslant O(1)$, where σ is the Prandtl number, have been worked out, with the aid of the narrow-gap approximation, and discussed in part 1 (Allen 1972).† The condition $\bar{S} \geqslant O(1)$ applies to most of the numerical solutions presented here and the results will be compared with the predictions of the linear theory.

The requirement that the flow be axisymmetric, as in the present case, is a strong restriction. It was felt that it might be of interest to extend these solutions to the study of three-dimensional flow fields, where, for example, the flow in the annulus would be three-dimensional because of non-axisymmetric driving or because of the development of non-axisymmetric flow instabilities. The choice of the numerical methods and the geometry used here was influenced by the idea of a future extension of this study to three-dimensional flows.

2. Formulation

We consider a viscous heat-conducting incompressible fluid which satisfies the Boussinesq approximation in a frame of reference rotating with uniform angular velocity $\boldsymbol{\Omega} = \Omega\hat{\mathbf{k}}$ and acted on by a gravitational acceleration $\mathbf{g} = -g\hat{\mathbf{k}}$

† In part 1, $\bar{S}$, because of its natural occurrence, was referred to as the stratification parameter. Here we use that designation for S.

which is antiparallel to the rotation vector. The governing equations are

$$\nabla . \mathbf{q} = 0,$$

$$\frac{\partial \mathbf{q}}{\partial t} + \mathbf{q} . \nabla \mathbf{q} + 2\Omega \hat{\mathbf{k}} \times \mathbf{q} = -\frac{\nabla p}{\rho_0} - \frac{\rho}{\rho_0} g \hat{\mathbf{k}} + \frac{1}{2} \frac{\rho}{\rho_0} \Omega^2 \nabla |\hat{\mathbf{k}} \times \mathbf{r}|^2 - \nu \nabla \times (\nabla \times \mathbf{q}),$$

$$\partial T / \partial t + \mathbf{q} . \nabla T = \kappa \nabla^2 T,$$

$$\rho = \rho_0 [1 - \alpha (T - T_0)],$$

where $\mathbf{q}, p, \rho$ and T are respectively the velocity, pressure, density and temperature of the fluid and are functions of position $\mathbf{r}$ and time t; ν, κ and α are respectively the constant kinematic viscosity, thermometric conductivity and coefficient of thermal expansion; ρ_0 and T_0 are constant reference values of the density and temperature; $\hat{\mathbf{k}}$ is a constant unit vector in the z direction in a cylindrical polar co-ordinate system (r, θ, z).

The variables are non-dimensionalized in the following manner:

$$\mathbf{q} = U \mathbf{q}^*, \quad \mathbf{r} = H \mathbf{r}^*, \quad t = \Omega^{-1} t^*,$$

$$p = p_0 - \rho_0 g H z^* + \tfrac{1}{2} \rho_0 \Omega^2 H^2 r^{*2} + \rho_0 U \Omega H p^*,$$

$$T = T_0 + \Delta T_0 T^*, \quad \rho = \rho_0 (1 + \alpha \Delta T_0 \rho^*),$$

where p_0 is a constant reference value of the pressure, U is a reference velocity and ΔT_0 is the basic temperature difference imposed over the height H of the annulus.

The resulting dimensionless equations are (dropping the asterisks)

$$\nabla . \mathbf{q} = 0, \tag{2.1a}$$

$$\partial \mathbf{q} / \partial t + \epsilon \mathbf{q} . \nabla \mathbf{q} + 2 \hat{\mathbf{k}} \times \mathbf{q} = -\nabla p - (S/\epsilon) \rho \hat{\mathbf{k}} + \tfrac{1}{2} (S/\epsilon) F \rho \nabla |\hat{\mathbf{k}} \times \mathbf{r}|^2 - E \nabla \times (\nabla \times \mathbf{q}), \tag{2.1b}$$

$$\partial T / \partial t + \epsilon \mathbf{q} . \nabla T = (E/\sigma) \nabla^2 T, \tag{2.1c}$$

$$\rho = -T, \tag{2.1d}$$

where $\epsilon = U/\Omega H$ is the Rossby number, $E = \nu/\Omega H^2$ is the Ekman number, $\sigma = \nu/\kappa$ is the Prandtl number, $F = \Omega^2 H/g$ is the rotational Froude number, $S = N^2/\Omega^2$ is the stratification parameter and $N^2 = \alpha g \Delta T_0 / H$ is the square of the Brunt–Väisälä frequency.

The standard annulus geometry is used. The axis of the annulus is aligned with the (vertical) rotation vector and is placed at the centre of rotation. The fluid is contained between two coaxial cylinders with inner and outer radii R_1 and R_2, respectively. The top and bottom surfaces are formed by parallel horizontal planes a distance H apart. The boundaries are all rigid surfaces. Cylindrical polar co-ordinates (r, θ, z) with unit vectors $(\hat{\mathbf{r}}, \hat{\boldsymbol{\theta}}, \hat{\mathbf{k}})$ are used, where the z axis coincides with the axis of the annulus. The origin of co-ordinates is placed in the plane of the bottom surface so that, in terms of the dimensionless variables, the fluid is contained in the region $(0 \leqslant z \leqslant 1, r_1 \leqslant r \leqslant r_2)$, where $r_1 = R_1/H$, $r_2 = R_2/H$. For this study we have chosen the relative dimensions to be

$$R_1 = R_2 - R_1 = H$$

so that the annulus has a square cross-section and $r_1 = r_2 - r_1 = 1$, $r_2 = 2$.

E	ϵ	S	σ	F	$r_1 (= R_1/H)$	$r_2 (= R_2/H)$
0·0005	0·01–0·2	0·0–3·0	7·0	0·0	1	2

TABLE 1. Range of parameters

The simplifying assumption that $F \ll 1$ has been made and the centrifugal force term in (2.1b) has been neglected by formally setting $F = 0$. A value for the Prandtl number $\sigma = 7$, which is close to that for water, was used. The Ekman number was chosen to be as small as was felt to be reasonable with the given grid spacing (see §6) and a single fixed value of $E = 0{\cdot}0005$ was employed. The values of the parameters S and ϵ were varied in the solutions. The range of the parameters is summarized in table 1.

The boundary conditions that are used for most of the solutions are

$$\mathbf{q}(z = 1) = -(r/r_2)\,\hat{\boldsymbol{\theta}}, \tag{2.2a}$$

$$\mathbf{q}(r = r_1) = \mathbf{q}(r = r_2) = \mathbf{q}(z = 0) = 0, \tag{2.2b}$$

$$T(z = 0) = 0, \quad T(z = 1) = 1, \tag{2.2c}$$

$$T_r(r = r_1) = T_r(r = r_2) = 0, \tag{2.2d}$$

where the subscripts denote partial differentiation.

Alternative boundary conditions, used in place of one of the above, are

$$\mathbf{q}(z = 1) = +(r/r_2)\,\hat{\boldsymbol{\theta}}, \tag{2.3a}$$

$$T_z(z = 0) = T_z(z = 1) = 1, \tag{2.3b}$$

$$\mathbf{q}_z(z = 1) = [C_1 + C_2(r - r_1)]\,\hat{\boldsymbol{\theta}}, \tag{2.3c}$$

$$T(r = r_1) = T(r = r_2) = z, \tag{2.3d}$$

where C_1 and C_2 are $O(1)$ constants. When conditions (2.3) are used, (2.3a) or (2.3c) replaces (2.2a), (2.3b) replaces (2.2c) and (2.3d) replaces (2.2d). In (2.3c) the motion is driven by an applied stress τ. In that case we assume $\tau = \tau_0 \tau^*$, where τ_0 is a reference value of the applied stress, and we define $U = H\tau_0/\rho_0\nu$ so that $\tau^* = \mathbf{q}_z^* \cdot \hat{\boldsymbol{\theta}}$. The choice of C_1 and C_2 is discussed in §4.3 (see (4.2)). When a fixed heat flux (2.3b) is employed as a boundary condition on the top and bottom surfaces, ΔT_0 designates the temperature difference applied between these surfaces when the fluid is in static equilibrium and $T_z \equiv 1$. We note that if $\Delta\Omega$ designates the relative angular velocity of the top surface then, with boundary condition (2.2a) on the velocity, we have $|\Delta\Omega|/\Omega = \epsilon(H/R_2) = \frac{1}{2}\epsilon$.

The finite-difference methods that have been used are those employed by Williams (1969, 1971) for the calculation of unsteady three-dimensional flows. The methods are discussed in the appendix. Approximate steady-state solutions (see §5) are obtained by integrating an initial-value problem forward in time from an initial condition of static equilibrium, $\mathbf{q} = 0$, $T = z$ (recall $F = 0$). The difference equations are written in cylindrical-polar co-ordinates, where the

standard notation (u, v, w) is used for the velocity components in the (r, θ, z) directions. A uniform rectangular grid with 50 and 64 cells between boundaries in the r and z directions is used. The solutions presented are not for a perfect steady state. The variables are still changing very slowly with increasing time. These changes are apparently governed by diffusive processes. The variables appear, however, to be close to their final steady values. This matter is discussed in detail in § 5. It is felt that the conclusions that will be drawn on the relative nature of the steady flow at different parameter values are not dependent on this lack of attainment of a perfect steady state.

3. Numerical solutions

A rough idea of the parameter values for which nonlinear effects can be expected to be important may be obtained from an order-of-magnitude analysis. For this purpose, it is convenient to make the substitutions

$$T = z + (\epsilon/S)\, T_p, \quad p = \tfrac{1}{2}(S/\epsilon)\, z^2 + p_p, \tag{3.1}$$

where T_p is the usual perturbation temperature in linear theory. Equation (2.1 *c*) then becomes, for steady axisymmetric flow,

$$\epsilon \mathbf{q} \,.\, \nabla T_p + Sw = (E/\sigma)\, \nabla^2 T_p, \tag{3.2}$$

where

$$\mathbf{q} \,.\, \nabla T_p = u(\partial T_p/\partial r) + w(\partial T_p/\partial z).$$

For $\epsilon \ll 1$, the governing equations for the linear theory are obtained, after substituting (3.1), by neglecting the terms multiplied by ϵ in (2.1 *b*, *c*). For increasing values of ϵ the neglected nonlinear terms will eventually become important. It turns out, with the moderately large value of the Prandtl number ($\sigma = 7$) used here, that nonlinear effects appear first in the energy equation (3.2). We therefore consider the relative size of the two terms on the left-hand side of (3.2):

$$L = O(\epsilon \mathbf{q} \,.\, \nabla T_p)/O(Sw). \tag{3.3}$$

According to linear theory for axisymmetric flow, with $\epsilon \ll 1$ and

$$O(E^{\frac{1}{2}}) < \tfrac{1}{4}\sigma S \leqslant O(1)$$

and with applied velocity driving, the variables in the interior have the scaling (Barcilon & Pedlosky 1967*b*) $v = O(1)$, $T_p = O(1)$, $u = O(E)$ and $w = O(E/\sigma S)$. As a result, we find (Pedlosky 1970) that $L = O(\epsilon/S)$ and therefore that the equations should be approximately linear if

$$\epsilon/S \ll 1. \tag{3.4}$$

Note that this is the same as the condition that is obtained by requiring that the magnitude of the total perturbation temperature in (3.1) be small compared with the $O(1)$ basic temperature. We remark, as is pointed out by Pedlosky (1970), that the above estimate is very much dependent on the fact that the flow is assumed to be axisymmetric. This is basically because for axisymmetric flow the convection terms are small, since $u \ll O(1)$ and $v(\partial/\partial\theta) \equiv 0$.

Solution	S	ϵ	Boundary conditions	t_B	t_A	$\psi_{\max} \times 10^3$
$S1$	0·0	0·1	(2.2)	133·76	110·03	14·87
$S2$	0·5	0·1	(2.2)	260·65	212·06	3·76
$S3$	1·1	0·1	(2.2)	277·05	205·03	2·71
$S4$	3·0	0·1	(2.2)	251·56	203·54	1·80
$S3A$	1·1	0·01	(2.2)	241·53	193·55	3·07
$S3B$	1·1	0·2	(2.2)	264·99	216·97	2·69
$S3C$	1·1	0·1	(2.3a)	240·09	194·46	6·30
$S3D$	1·1	0·1	(2.3b)	216·06	167·09	3·44
$S3E$	1·1	0·1	(2.3c)	311·33	263·33	1·39
$S3F$	1·1	0·1	(2.3d)	220·87	171·34	5·72

TABLE 2. A list of the solutions, with the values of the parameters ϵ and S and the boundary conditions. t_B is the elapsed dimensionless time from the start of the initial-value problem. t_A is an intermediate time that is discussed in §5. $\psi_{\max}$ is the maximum absolute value of the stream function, at t_B, with $\psi = 0$ on the boundaries.

For stratifications in the range $O(1) \leqslant \frac{1}{4}\sigma S \leqslant O(E^{-1})$, a different estimate is obtained. The interior variables have the scaling (Allen 1972) $v = O(1), T_p = O(1)$, $u = O(E\sigma^{\frac{1}{2}}S^{\frac{1}{2}})$ and $w = O(E)$. This leads to $L = O(\epsilon\sigma^{\frac{1}{2}}S^{-\frac{1}{2}})$ and therefore to the following condition for approximate linearity:

$$\epsilon\sigma^{\frac{1}{2}}S^{-\frac{1}{2}} \ll 1. \tag{3.5}$$

One of the purposes of this study is to calculate solutions with values of ϵ that are large enough for nonlinearities to be important. The estimates (3.4) and (3.5) indicate that for $S > O(1)$, and $\sigma \geqslant O(1)$ the effects of stratification, combined with the geometrical restriction to axial symmetry, apparently maintain linearity for finite values of ϵ. An additional consideration in choosing values of ϵ, however, involves the question of the possible instability of a real flow to non-axisymmetric disturbances. In fact, the flows studied here can be expected to be susceptible, for increasing values of ϵ, to the onset of baroclinic instability. For $\sigma S < O(1)$, that problem has been studied by Pedlosky (1970).

On the question of stability for $\sigma S \geqslant O(1)$, there is, to our knowledge, no guidance available at the present from linear stability analyses or from laboratory experiments. In order to strike a balance, then, between a desire to study nonlinear effects due to substantial values of ϵ and the desire to calculate solutions which have some chance of being stable axisymmetric flows, the bulk of the solutions were calculated at the moderate value of $\epsilon = 0{\cdot}1$. As will be discussed in §4, for applied velocity driving nonlinear effects appear with this choice of ϵ, even though it is smaller than that indicated by (3.5). This is apparently related to the specific nature of the flow generated by the non-zero values of the applied velocity at r_1 and r_2.

The solutions that have been calculated are listed in table 2 with the corresponding values of the parameters S and ϵ and with the boundary conditions. The dimensionless time t_B, which is the elapsed time from the start of the initial-value problem, is also given. Solutions $S1$–$S4$ form a set where S is varied with ϵ

held fixed at $\epsilon = 0{\cdot}1$, whereas in solutions $S3$, $S3A$ and $S3B$, ϵ is varied, with S held fixed at $S = 1{\cdot}1$. In all of these cases the boundary conditions (2.2) are used. In solutions $S3C$–F, ϵ and S are fixed at $\epsilon = 0{\cdot}1$ and $S = 1{\cdot}1$ and the boundary conditions are varied. Conditions (2.3*a*–*d*) are used in place of the appropriate condition in (2.2).

4. Discussion of solutions

The general features of the solutions can be seen most easily from contour plots of the zonal velocity field v, the temperature field T and the stream function ψ for the meridional circulation. The stream function is defined such that $ru = \psi_z$ and $rw = -\psi_r$ and is obtained by numerical integration of the velocity component u. Contour plots of v, T and ψ in the annulus cross-section

$$(1 \leqslant r \leqslant 2,\ 0 \leqslant z \leqslant 1)$$

for the solutions in table 2 at times t_B are presented in figure 1. The outer side wall ($r = 2$) is on the right-hand side of the plots.

4.1. *Variation of S*

Solutions $S1$–$S4$ are shown in figures 1 (*a*)–(*d*). In this set of solutions the Rossby number ϵ is held fixed ($\epsilon = 0{\cdot}1$) and the stratification parameters S is varied. In $S1$ there is no stratification, $S = 0$, and the fluid is homogeneous. An investigation of the relative size of the terms in the numerical solution shows that the dynamics is governed by the balances of linear theory (Greenspan 1968, §§ 2.17–18). This is expected since $\epsilon < E^{\frac{1}{2}}$ (see Barcilon 1970).

Results which are familiar from linear theory are evident in the solution. The plot of v shows the adjustment of the interior zonal velocity to the velocity of the boundaries through thin Ekman layers on the top and bottom surfaces and through thicker boundary layers on the side walls. It also shows the z independence of v in the interior. The plot of ψ shows a meridional flow which circulates from one Ekman layer to the other, through the interior and the side-wall boundary layers. The flow is upward, from the bottom surface to the top, in the outer side-wall boundary layer and downwards elsewhere. The almost vertical alignment of the streamlines in the interior reflects again the z independence of the interior motion. The circulation in the boundary layer on the outer side wall has

---

FIGURE 1. Contour plots of the zontal velocity field v, the temperature field T, and the stream function ψ in the annulus cross-section ($1 \leqslant r \leqslant 2$, $0 \leqslant z \leqslant 1$) for the solutions in table 2 at times t_B. The outer side wall ($r = 2$) is on the right-hand side of the plots. With the exceptions noted below, the maximum and minimum values in the field and the intervals at which the contours are plotted are $v_{\max} = 0$, $v_{\min} = -1{\cdot}0$, $\Delta v = 0{\cdot}1$, $T_{\max} = 1{\cdot}0$, $T_{\min} = 0$, $\Delta T = 0{\cdot}1$, $|\psi|_{\max}$ as in table 2, $\psi_{\min} = 0$, $\Delta\psi = 0{\cdot}1|\psi|_{\max}$. For (*g*), $S3C$, $v_{\max} = 1{\cdot}0$, $v_{\min} = 0$, $\Delta v = 0{\cdot}1$. For (*h*), $S3D$, $T_{\max} = 1{\cdot}084$, $T_{\min} = -0{\cdot}015$, $\psi_{\min} = -2{\cdot}88 \times 10^{-6}$; contours are plotted at intervals of $\Delta T = 0{\cdot}110$ starting at $T = 0$ and at intervals of $\Delta\psi$ starting at $\psi = 0$. For (i) $S3E$, $v_{\max} = 0$, $v_{\min} = -0{\cdot}498$; contours are plotted at intervals of $\Delta v = 0{\cdot}1$ from $v = -0{\cdot}1$ to $-0{\cdot}4$. The occasional breaks in the contour lines are due to misfunctions in the plotting routine.

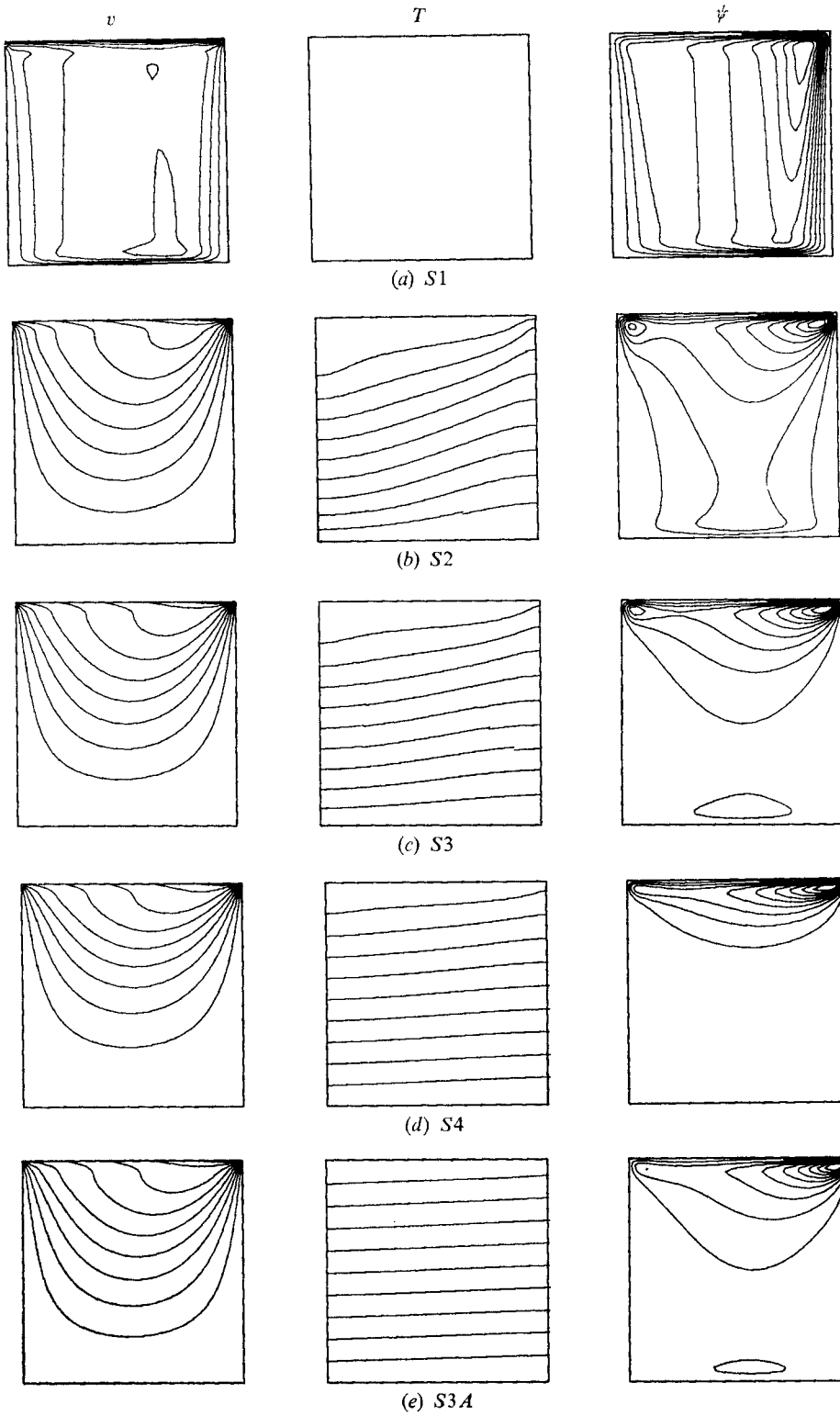

FIGURES 1(a)–(e). For legend see p. 343.

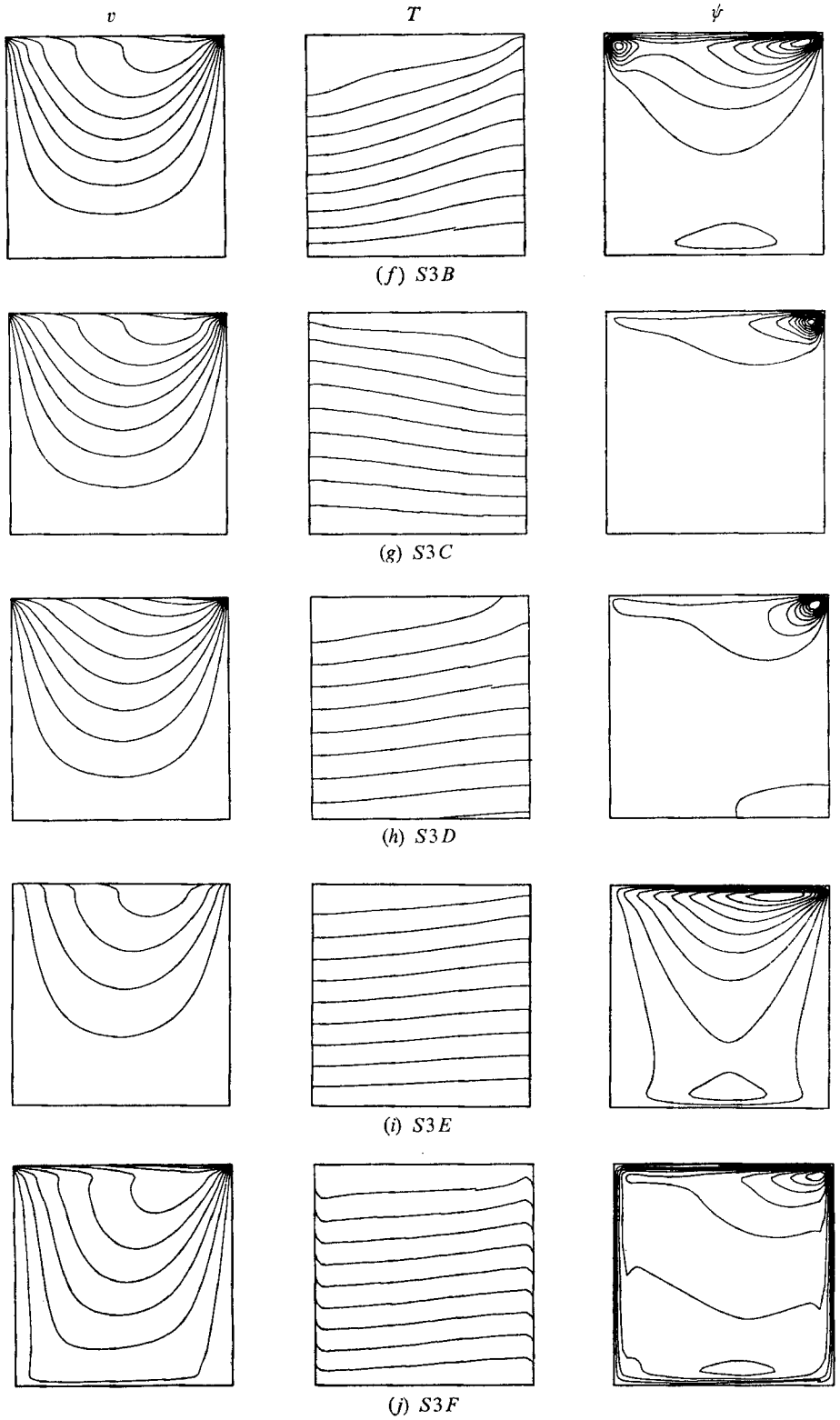

(*f*) *S*3*B*

(*g*) *S*3*C*

(*h*) *S*3*D*

(*i*) *S*3*E*

(*j*) *S*3*F*

FIGURES 1(*f*)–(*j*). For legend see p. 343.

the same general form as that found from the solutions of the $E^{\frac{1}{4}}$ and $E^{\frac{1}{3}}$ layers of linear theory. It is predicted there, for this problem, that fluid will enter the $E^{\frac{1}{4}}$ layer on the outer side wall from the Ekman layer on the bottom surface. Fluid also enters the $E^{\frac{1}{4}}$ layer from the Ekman layer on the top surface. Both contributions flow from the $E^{\frac{1}{4}}$ layer towards the wall to the $E^{\frac{1}{3}}$ layer and are transported to the Ekman layer on the top surface through an $E^{\frac{1}{2}} \times E^{\frac{1}{2}}$ corner region. The flow near the outer side wall in figure 1(*a*) can be seen to have this general character. The predicted thickness of the $E^{\frac{1}{4}}$ layer is $\delta \simeq 2E^{\frac{1}{4}} \simeq 0{\cdot}3$ and this is approximately the thickness found from the numerical solution. The accuracy of the resolution of the solution in the Ekman layers will be discussed in §6.

The maximum value of ψ, with $\psi = 0$ on the boundaries, gives an indication of the strength of the meridional, or upwelling, circulation. These values are recorded, for all the solutions, in table 2. The relative values of $\psi_{\max}$ will be compared to give an indication of the effects of stratification and of different boundary conditions on the upwelling circulation.

In solution $S2$ the value of S is increased to $S = 0{\cdot}5$. Note that, according to linear theory (Barcilon & Pedlosky 1967*a*), this is a case of substantial stratification, since $\frac{1}{4}\sigma S = 0{\cdot}875 = O(1)$. In the plot of v (figure 1*b*) it can be seen that the interior zonal velocity is now very much z-dependent, and that it adjusts smoothly, with no boundary-layer structure, to the side-wall values. As is verified by an examination of the relative size of the terms in the equations, the interior flow is characterized by a geostrophic and hydrostatic balance which results in the satisfaction of the 'thermal wind' relation

$$v_z = \tfrac{1}{2}(S/\epsilon)\, T_r. \tag{4.1}$$

The horizontal gradients of temperature can be seen in the plot of T. There is an Ekman layer on the top surface as shown by the balance of terms in the solution. This can also be seen in the contour plots from the adjustment of v to the interior values and from the concentrated meridional transport next to the top surface. Evidence of a much weaker Ekman layer on the bottom surface can also be seen in the plot of ψ from the crowding of streamlines near that surface.

The nature of the flow is changed appreciably from that in the unstratified case $S = 0$. The meridional circulation is still characterized by a concentrated upwelling into the top-surface Ekman layer at the outer side wall and by a corresponding downwelling at the inner side wall. However, fluid is now fed to the upwelling corner directly from the interior and there is no involvement of the flow in side-wall boundary layers. The circulation to and from the top-surface Ekman layer is completed through the interior and a much weaker Ekman layer on the bottom surface. The effects on the temperature field of the upwelling and downwelling can be clearly seen in the plot of T from the convective distortion of the isotherms near the top corners. The maximum value of the stream function is about one-quarter of that in $S1$, which shows that the stratification has substantially reduced the magnitude of the meridional circulation.

The stratification is increased further to $S = 1{\cdot}1$ in solution $S3$ (figure 1*c*). In the plots of v and ψ, it can be seen that the Ekman layer remains on the top

surface but that it is weaker than in case $S2$. This is roughly illustrated by the decrease in length of the nearly horizontal portion of the contour lines of v next to the top surface. The plot of T shows the interior, 'thermal wind', temperature gradients and the effects of upwelling and downwelling in the top corners. Compared with $S2$, the increased stratification has led to a general decrease in the magnitude of the gradients in the dimensionless temperature. This is anticipated from the scaling of the perturbation temperature in linear theory (3.1) by the factor ϵ/S. The meridional circulation has crowded closer to the top surface than in $S2$, and is seen to be dominated by relatively intense eddies in the upwelling and downwelling corners. The strength of the meridional circulation has decreased further and $\psi_{\max}(S3) = 0{\cdot}18\psi_{\max}(S1)$. As will be discussed shortly, an examination of the size of the terms in the energy equation (2.1*c*) shows that nonlinear effects are important near the upwelling corner.

In solution $S4$ (figure 1*d*) the stratification is increased to $S = 3{\cdot}0$. The same trends, as shown in the differences between $S2$ and $S3$, continue. The Ekman layer on the top surface is weakened. The general depth of penetration of the applied velocity and the magnitude of the temperature gradients have decreased. The meridional circulation is completed very close to the top surface and has approximately one-eighth the strength of the circulation with $S = 0$, i.e. $\psi_{\max}(S4) = 0{\cdot}12\psi_{\max}(S1)$.

Solutions $S1$–$S4$ show the strong effect of stratification on the general nature of the flow and, in particular, on the meridional circulation. General results from the linear theory of Barcilon & Pedlosky (1967*a*), such as the decrease in strength of the surface Ekman layers and the vertical velocities, are illustrated. Specific predictions made in part 1 are also shown. In particular, the general form of the zonal velocity, outside the top-surface Ekman layer, was well illustrated there even with the assumption of an infinite-depth annulus. The nature of the meridional circulation, with eddies in the upper corners, was also predicted. The linear theory also indicated that the meridional circulation would be confined to a Lineykin layer of thickness of $O(\bar{S}^{-\frac{1}{2}})$ and that therefore the circulation would crowd closer to the top surface as the stratification was increased. This result is clearly illustrated in the numerical solutions.

The strength of the upwelling circulation, as measured by $\psi_{\max}$, decreases sharply in the numerical solutions with increasing values of S. In part 1 the dependence of $\psi_{\max}$ on the parameters E and $\bar{S}$ was estimated from scaling arguments regarding the corner region and the result was $\psi_{\max} \sim O[(E^{\frac{1}{2}}\bar{S}^{-\frac{1}{2}}(1+\bar{S}^{-\frac{1}{2}})]$. If we compare the results of this estimate, which gives $R = \psi_{\max}(S4)/\psi_{\max}(S3) = 0{\cdot}505$, with the results of the numerical solutions, from which we find $R = 0{\cdot}664$, we see that, although the trend is correct, the agreement is not that close. The fact that nonlinear effects are important near the corners and, as shown below, affect the value of $\psi_{\max}$, probably influences the value of R from the numerical solutions and precludes a useful comparison.

4.2. *Variation of* ϵ

In solutions $S3$, $S3A$ and $S3B$ the stratification is held fixed at $S = 1{\cdot}1$ while the value of the Rossby number is varied. In $S3A$ (figure 1*e*) a relatively small value of the Rossby number, $\epsilon = 0{\cdot}01$, is used. An examination of the relative size of the terms in the equations shows that this solution is governed by the balances of linear theory. We note that the zonal velocity v has approximately the same distribution as in $S3$. The interior horizontal temperature gradients are smaller in $S3A$, however, as is expected from the coefficients in the 'thermal wind' relation (4.1). There is also appreciably less distortion, relative to the interior, of the isotherms in the upwelling and downwelling corners. We also note that $\psi_{\max}(S3)$ is smaller than $\psi_{\max}(S3A)$. ψ is a dimensionless stream function and the values would remain unchanged if the two solutions obeyed linear equations. The maximum meridional transport goes through the upwelling corner and the decrease in $\psi_{\max}$, in $S3$, is probably due to the increase of the vertical temperature gradients in this region caused by the convective effects of the upwelling velocities and the fixed temperature boundary condition at the top surface. This increase in the local stratification in the upwelling corner apparently decreases the total meridional transport. It can also be seen that the local downwelling at the inside corner is stronger in $S3$ than in $S3$A and this is probably due to the fact that the local stratification is weaker there in $S3$.

The same trends that were evidenced in the change from $S3A$ to $S3$ continue with the further increase of the Rossby number to $\epsilon = 0{\cdot}2$ in $S3B$ (figure 1*f*). $\psi_{\max}(S3B)$ is just slightly less than $\psi_{\max}(S3)$ but, as can be seen in the plot of ψ, the magnitude of the downwelling is increased considerably in $S3B$. There is also now a significant horizontal temperature gradient in the interior and larger convective distortion of the isotherms in the upper corners.

4.3. *Variation of boundary conditions*

In solutions $S3C$–F (figures 1*g*–*j*) the values of S and ϵ are fixed at the same values as in $S3$, i.e. $S = 1{\cdot}1$ and $\epsilon = 0{\cdot}1$, but the boundary conditions are changed.

In $S3C$ (figure 1*g*) the rotation of the top surface (2.3*a*) has the same magnitude as in $S3$, but is in the opposite direction. As a result, the direction of the zonal velocity and the meridional circulation is reversed. There is now downwelling at the outer corner. These effects are easily seen from the slope of the isotherms in the temperature plot. The character of the meridional circulation is changed appreciably compared with that in $S3$. Note that, if the solutions were linear, the streamlines would have the same pattern in both cases. The magnitude of the meridional circulation is increased in $S3C$, i.e. $\psi_{\max}(S3C) = 2{\cdot}32\psi_{\max}(S3)$. Apparently, the local stratification near the outer corner is reduced considerably by the downwelling and as a result there is a relatively intense recirculating eddy in this region of decreased temperature gradient. A corresponding decrease in v_z, compared with that in $S3$, is also noticeable in this region.

In solution $S3D$ (figure 1*h*) the constant-temperature boundary condition on the top and bottom surfaces is replaced by one of a constant heat flux (2.3*b*). With a boundary condition on the heat flux, the isotherms can, of course,

intersect the top surface and, evidently, as a result there are weaker temperature gradients in the upwelling corner. The pattern of the upwelling circulation is different from that in $S3$. The circulation is stronger here, i.e. $\psi_{\max}(S3D) = 1{\cdot}27\psi_{\max}(S3)$, and most of the flow is concentrated in the upwelling corner. There is less transport in the top-surface Ekman layer. In fact, as can be seen from a comparison of the change in vertical gradients of v near the top surface, the Ekman layer is substantially weaker in this case. Since horizontal gradients of temperature are possible at the top surface, whereas with a fixed constant surface temperature they are not, the interior flow, which obeys the 'thermal wind' equation, can itself have larger vertical gradients of zonal velocity there. The weakening of the top-surface Ekman layer, compared with the fixed temperature case $S3$, was predicted by linear theory in part 1. It was also predicted there, however, that the magnitude of the meridional transport would decrease by a factor of $\bar{S}^{-\frac{1}{2}}$ compared with case $S3$. The fact that the transport increases here can be attributed to the nonlinear behaviour of the flow in the top corner regions. In the bottom corner, by the outer side wall, there is a region of very weak meridional flow which is circulating in a direction opposite to that of the main upwelling motion.

In solution $S3E$ (figure 1*i*) the driving mechanism of an applied velocity at the top surface is changed to an applied stress (2.3*c*). In an attempt to get a solution which would be comparable with $S3$, the magnitude of the applied stress in $S3E$ was determined by taking the final computed values of v_z ($r = 1{\cdot}47$, $z = 1$) and v_{zr} ($r = 1{\cdot}47$, $z = 1$) from solution $S3$ and choosing C_1 and C_2 in (2.3*c*) so that the applied stress v_z, which is linear in r, would have these same values. The result is that $C_1 = -1{\cdot}27$ and $C_2 = -3{\cdot}23$ and

$$v_z(z = 1) = -1{\cdot}27 - 3{\cdot}23(r-1), \quad u_z(z = 1) = 0. \tag{4.2}$$

Note that the applied stress is non-zero at both r_1 and r_2 and that the maximum absolute value is $|v_z(r = r_2, z = 1)| = 4{\cdot}5$.

In the stress-driven case $S3E$ the meridional circulation is still characterized by upwelling from the interior into the top-surface Ekman layer at the outer side wall. The general qualitative features of the flow are not greatly different from those in $S3$. The region of upwelling, however, is spread out over a larger distance from the corner in this case than it was with the applied velocity driving. The change in slope of the isotherms in the upwelling region, relative to that in the interior, also appears to be less here, presumably corresponding to the weaker upwelling velocities and the more diffuse region of upwelling. Direct comparisons of the two cases are hard to make since the Rossby numbers based on local values differ. It does appear, however, that an applied velocity driving with a non-zero value at the side wall results in an upwelling flow which is more concentrated toward the corner than is the case with an applied stress which also has a non-zero value at the side wall.

In $S3E$ there is a relatively uniform rate of outflow from the top-surface Ekman layer to the interior, as evidenced by the regular spacing of streamlines in that region. This is predicted, for this stratified problem (part 1), by Ekman-layer theory and is a result, of course, of the linear variation of the

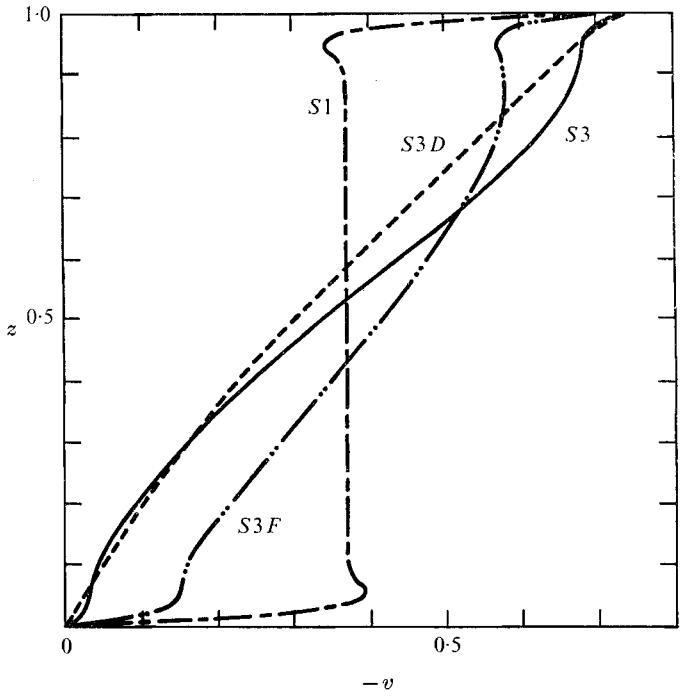

FIGURE 2. Profiles of the zonal velocity v at times t_B, from the solutions $S1$, $S3$, $S3D$ and $S3F$, along $r = 1{\cdot}49$.

applied stress. We note that the outflow from the Ekman layer in the applied velocity case is different because it is not directly related, in the same manner as it is in a homogeneous fluid, to the functional form of the applied velocity and the interior vorticity (see part 1). The maximum absolute value of v appears at the top surface at $r = 1{\cdot}69$, $z = 1$ and is $|v|_{\max} = 0{\cdot}498$.

In solution $S3F$ (figure 1j) the temperature boundary condition at the side wall is changed from one of no heat flux to one where the temperature is held fixed at the initial value $T = z$, equation (2.3d). The character of the flow that results is appreciably different from that in $S3$, where the side walls are thermally insulated. There is a relatively strong Ekman layer on the top surface here. The values of the zonal velocity in the bottom part of the interior are larger than in $S3$ and there is an Ekman layer on the bottom surface. A substantial portion of the meridional circulation is completed entirely in boundary layers. This flow circulates through Ekman layers on the top and bottom surfaces and through thin boundary layers on the side walls. An examination of the terms in the equations shows, as is expected from the linear-theory results of Barcilon & Pedlosky (1967a), that the balance in these side-wall layers is that of the buoyancy layer. The rest of the meridional transport is completed in the interior with again an eddy type of motion near the upwelling corner. The strength of the meridional circulation is about twice that in $S3$, i.e. $\psi_{\max}(S3F) \simeq 2{\cdot}1\psi_{\max}(S3)$. The temperature plot shows the slope of the isotherms in the interior and the return of the temperature, in the side-wall buoyancy layers, to the specified values at the wall.

The effect of convection in the side-wall boundary layers, near the upwelling and downwelling corners, is also evident from the shape of the isotherms there.

In figure 2, the zonal velocity v from solutions $S1$, $S3$, $S3D$ and $S3F$ is plotted as a function of z along the line $r = 1{\cdot}49$. Several of the features that were noted from the contour plots are shown clearly here. The solution for v from $S1$, for which $S = 0$, exhibits a z-independent behaviour in the interior and rapid variations in Ekman layers at the top and bottom surfaces. For $S3$, there is a relatively continuous variation of v with z. There are signs of weak Ekman layers at the surfaces. Near the top and bottom, the profile has regions where v_z is relatively small. This is apparently a result of the constant temperature boundary condition on the top and bottom surfaces and the satisfaction of the 'thermal wind' relation (4.1) by the interior flow. This region of small v_z is absent in the profile of v from $SD3$, where there is a fixed heat flux boundary condition on the horizontal surfaces. In that profile, there appears to be only an extremely small adjustment of the interior flow to the surface values in boundary layers. The profile from $S3F$, where the side-wall temperature is specified, shows much stronger Ekman layers, compared with $S3$, at both surfaces and, consequently, a generally smaller gradient of v in the interior. Regions near the top and bottom where v_z is relatively small are evident here also.

4.4. *Relative size of terms*

More information on the nature of the flow in the solutions is available from a comparison of the relative sizes of the terms in the equations. Several conclusions that have been reached with this procedure have already been mentioned. Some illustrative, specific comparisons are presented below.

A useful equation to examine is that for the component of vorticity $\zeta_{(\theta)} = u_z - w_r$, in the azimuthal direction:

$$[\partial\zeta_{(\theta)}/\partial t] + \epsilon[(D(u) - r^{-1}v^2)_z - D(w)_r] - 2v_z + (S/\epsilon)\,T_r - E[J(u)_z - (\nabla^2 w)_r] = 0. \quad (4.3)$$

$$(a) \qquad (b) \qquad (c) \quad (d) \qquad (e)$$

The notation is defined in the appendix. This equation is derived in finite-difference form directly from the difference equations for u and w. In figure 3 the terms (a)–(e) in (4.3) are plotted for solution $S3$ along the line $r = 1{\cdot}47$. It can be seen that the interior is characterized by a balance of terms (c) and (d) which represents the 'thermal wind' equation (4.1). At a distance of approximately $\delta_z \simeq 0{\cdot}1$ from both the top and the bottom surface the viscous term (e) starts to increase in magnitude. Closer to the boundaries, the primary balance is that of terms (c) and (e). This reflects the Ekman-layer nature of the flow in this region next to the boundaries as can be verified from a comparison of the terms in the individual momentum equations. The nonlinear convection term (b) is relatively small throughout. The unsteady term (a) is not plotted, since it lies right along the zero line. The magnitude of (a) is typically about 10^{-5} times the dominant terms. The vorticity equation (4.3) is thus well characterized by a quasi-steady balance.

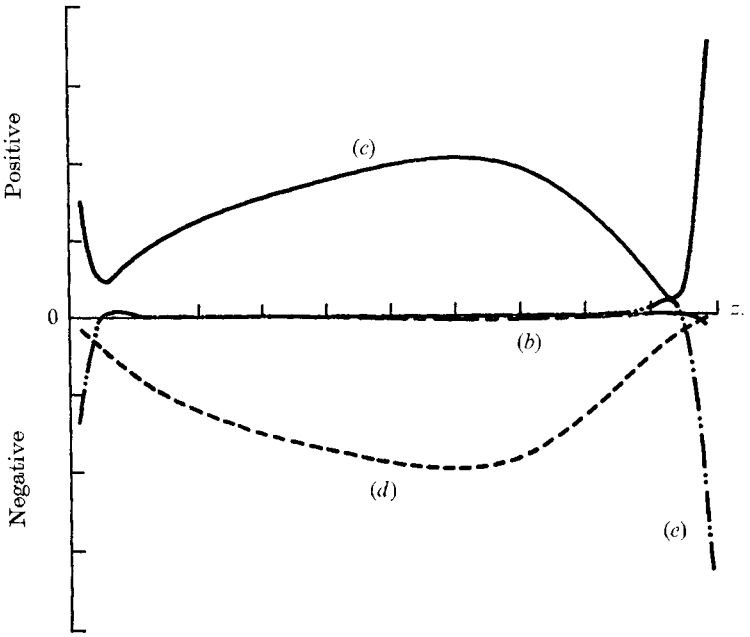

FIGURE 3. Terms in the vorticity equation (4.3) at time t_B, from solution $S3$, along $r = 1{\cdot}47$.

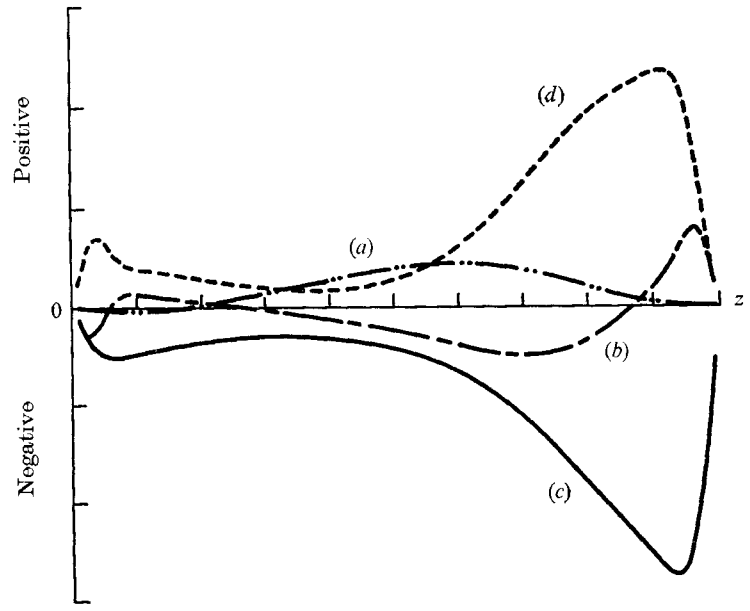

FIGURE 4. Terms in the energy equation (4.4) at time t_B, from solution $S3$, along $r = 1{\cdot}47$.

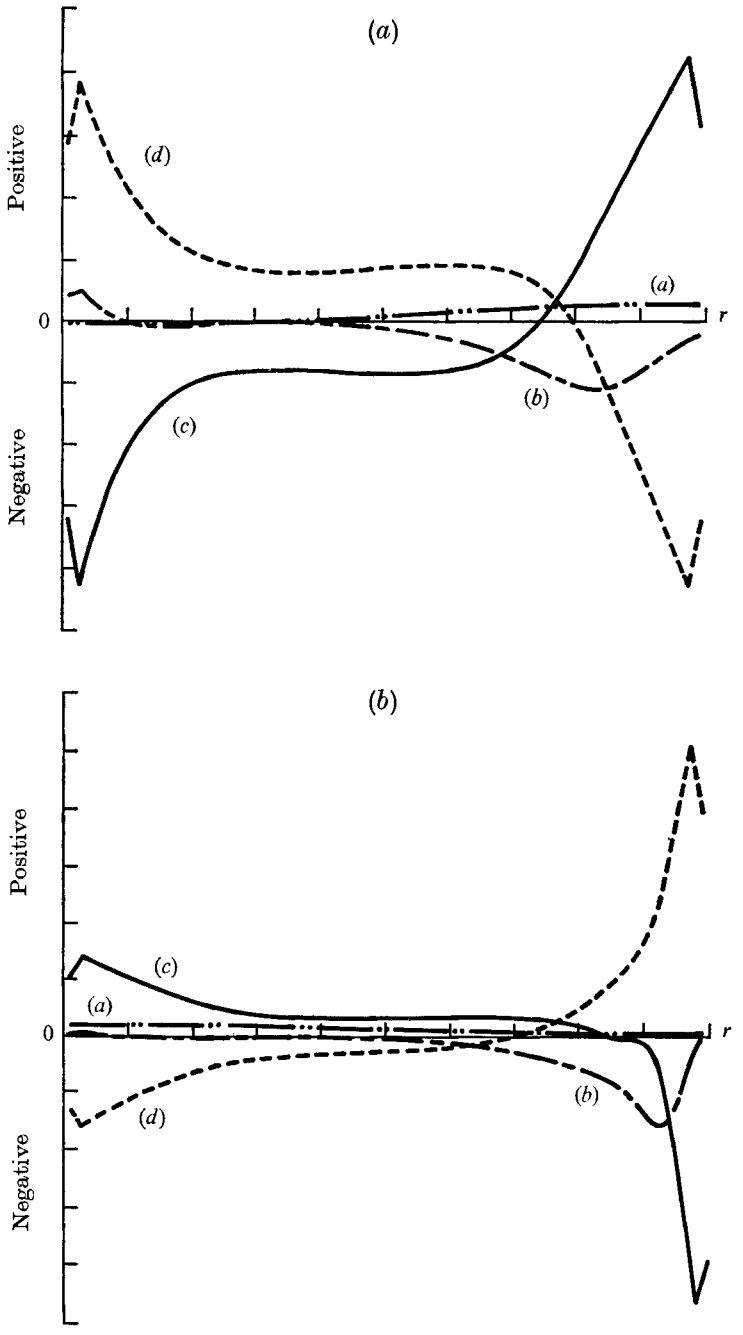

FIGURE 5. Terms in the energy equation (4.4) at times t_B, (*a*) from solution $S3$ and (*b*) from solution $S3C$, along $z = 0{\cdot}836$.

In figures 4 and 5, terms in the energy equation (2.1 c) are plotted. The balances in this equation are of interest because they show the nonlinear effects and also the extent of the unsteadiness that remains in the solutions. To show clearly the balance of linear theory, when it exists, (2.1 c) is written in the form

$$T_t + \epsilon[D(T) - w] + \epsilon w = (E/\sigma)\nabla^2 T \tag{4.4}$$

$$(a) \qquad (b) \qquad (c) \qquad (d)$$

and the values of the terms (a)–(d) are plotted.

In figure 4 the terms in (4.4) from solution $S3$ are plotted along the line $r = 1{\cdot}47$. This plot shows that the unsteady term (a) is relatively small near the boundaries but that it is not small in the interior. Near the centre of the annulus cross-section, (a) is primarily balanced by term (c), involving the vertical velocity. The magnitudes of the vertical velocities in the interior are, however, so small ($w(r = 1{\cdot}49, z = 0{\cdot}5) = -1{\cdot}4 \times 10^{-4}$) that the time rate of change of the temperature field is also very small. In the upper portion of the annulus, $z > 0{\cdot}7$, the balance is primarily between terms (c) and (d). This is the balance of linear theory for steady flow. A further breakdown of the heat conduction terms (d) shows that the major contribution for $z \geqslant 0{\cdot}7$ is from T_{zz}. This is expected from the analysis in part 1, which showed that term (c) would be balanced by T_{zz} in a Lineykin layer near the top surface. Right next to the top surface, $z \geqslant 0{\cdot}9$, the relative value of the nonlinear term (b) increases. Here, however, the flow is governed primarily by Ekman-layer balances and the temperature field is effectively uncoupled from the dynamics.

In figure 5(a) the terms in (4.4) from $S3$ are plotted along $z = 0{\cdot}836$, which is across the upper portion of the annulus. The relative magnitude of the unsteady term (a) is fairly small here. In the interior, towards the inner wall $1{\cdot}1 \leqslant r \leqslant 1{\cdot}6$, the balance is between the linear terms (c) and (d). However, near the outer wall in the upwelling region (where the value of (c) is positive), the nonlinear term (b) is important. An examination of the terms in the vorticity equation (4.3) in this region shows that the 'thermal wind' relation (4.1) holds and therefore that the nonlinearities in the energy equation (4.4) are coupled with the dynamics. It is interesting to compare this plot for $S3$ with a corresponding one for $S3C$ (figure 5b), where there is downwelling at the outer wall. It can be seen that the nonlinear term is relatively larger and more important in the downwelling case. This is presumably related to the stronger meridional circulation in $S3C$. It can also be seen, from term (c), that the downwelling is concentrated closer to the wall than was the upwelling in $S3$. The relative magnitude of the nonlinear terms shows an increase, for both solutions, if the value of z along which the terms are plotted is increased to $z = 0{\cdot}914$.

It is useful to compare qualitatively the magnitudes of the nonlinear effects in the other solutions. We do this by mentioning the differences shown in the plots, corresponding to figure 5, of the terms in (4.4) along $z = 0.836$. The plot for $S3B$, the case of largest Rossby number, shows features similar to those in figure 5(a) for $S3$, but the relative magnitude of the nonlinear term is increased considerably in the upwelling region and is much larger at the inner wall in the

downwelling region. In the linear solution $S3A$, the nonlinear term (b) is, of course, relatively small across the entire cross-section.

As the stratification is increased in solutions $S2$–$S4$, the relative magnitude of the nonlinear term (b) in the upwelling region, at the point of its maximum absolute value, appears to decrease. The relative size of (b) in the downwelling region also decreases. This apparently is a result of the general reduction in strength of the meridional circulation by increased stratification. A comparison with $S3$ of the fixed heat flux case $S3D$ shows that the relative magnitude of the nonlinear term (b) is much larger in $S3D$. This is presumably related to the weaker local stratification and stronger upwelling in that case. In the stress-driven solution $S3E$, the relative value of (b) is much smaller than in $S3$ and this is probably due to the fact that the upwelling is weaker and more diffuse in $S3E$. In $S3F$, the nonlinear effects are not noticeable at this value of z, where the upwelling flow is mainly confined to a thin side-wall boundary layer and the linear terms (c) and (d) balance

We have seen, in the applied-velocity-driven cases, that nonlinear effects in the energy region (2.1c) are important in the upwelling region at Rossby numbers ϵ of 0·1 and 0·2, although the order-of-magnitude analysis in § 3 gave no indication that this would be the case. The nonlinear effects are presumably related to the specific nature of the flow caused by an applied velocity boundary condition with non-zero values at the corners. This behaviour might have been anticipated from an examination of the linear-theory solutions in part 1, since they exhibit singular behaviour in the meridional velocity components u and w at a corner where the applied velocity is non-zero.

The linear-theory solutions may be used to check the relative magnitude of the neglected nonlinear terms in (2.1c) as the corner is approached. Let us consider a specific case from part 1 with boundary conditions similar to (2.2) (i.e. in the notation of that paper, solutions (3.14) and (3.16) with $D_0 = 1$ and $D_1 = -1$). The narrow-gap approximation is used there and the Cartesian co-ordinates (x, z) replace (r, z). If we examine the values of the ratio of terms

$$L = (b)/(c) = \epsilon \mathbf{q} \cdot \nabla T_p / Sw = \epsilon(uT_{px} + wT_{pz})/Sw$$

along the line $1-x = \alpha(1-z) = \eta$, which goes through the upwelling corner $(x = 1, z = 1)$, we find, for $\eta \ll 1$,

$$L \simeq \frac{\epsilon 4\bar{S}(1+\bar{S}^{-\frac{1}{2}})(1-3\bar{S}\alpha^{-2})}{\eta S\pi\alpha(1+\alpha^{-2})(1+\bar{S}\alpha^{-2})(\bar{S}\alpha^{-2}-1)}.$$

L increases as η decreases and the nonlinear terms increase in relative magnitude as the corner is approached. If we choose $\alpha = \frac{1}{2}\bar{S}^{\frac{1}{2}}$ ($w \equiv 0$ for $\alpha = \bar{S}^{\frac{1}{2}}$) so that the line is located in the upwelling part of the Lineykin layer, we find that $|L| \simeq 1$ for

$$\eta_0 \simeq \frac{\epsilon\sigma(1+\bar{S}^{-\frac{1}{2}})}{\pi\bar{S}^{\frac{1}{2}}(1+4\bar{S}^{-1})} 1{\cdot}47.$$

For the values of the parameters in $S3$, this gives $\eta_0 \simeq 0{\cdot}13$. We do not attach much significance to the exact value of η_0 here, but we do think the general result

that the nonlinear terms increase in relative magnitude as the corner is approached and the order of magnitude of η_0 are probably indicative of the flow behaviour. A corresponding comparison should be made for the terms in the v momentum equation (A 1c), i.e. for $L_v = \epsilon(uv_x + wv_z)/2u$. We find that

$$L_v \simeq \frac{\epsilon(1+\bar{S}^{-\frac{1}{2}})(1-3\bar{S}\alpha^{-2})}{\eta 2\pi\alpha(1+\alpha^{-2})(1+\bar{S}\alpha^{-2})}.$$

For $\alpha = \frac{1}{2}\bar{S}^{\frac{1}{2}}$, $|L_v|/|L| \simeq 1{\cdot}5/\sigma$ and for $S3$, $|L_v| \simeq 1$ for $\eta_{0v} \simeq 0{\cdot}028$. In the numerical solutions there was effectively no indication of nonlinearity in the v momentum equation. The nonlinear term was negligibly small just about everywhere. Very high in the upwelling corner, along $z = 0{\cdot}914$, it increased somewhat, but was still small relative to the other terms.

5. Approximate steady-state solutions

As we have mentioned, the solutions presented are not for a perfectly steady-state situation. The variables are still changing slowly with time. We have called these solutions 'approximate steady-state' solutions. The intended meaning of that terminology is that the solutions are sufficiently close to a steady state that information of interest on the relative nature of the steady solutions, at different parameter values, can be extracted. We discuss this matter in more detail below.

The solutions were obtained by numerically integrating an initial-value problem forward in time from an initial condition of static equilibrium, $\mathbf{q} = 0$, $T = z$ (with the exception of $S3B$, for which $S3$ at $t = t_A$ was the initial condition). The solutions were integrated to the dimensionless times t_A (table 2) at which point it appeared that an approximate steady state had been reached. At that point, however, a small $O(\Delta r)$ (see appendix) error in the application of the boundary condition on v at the inner side wall $r = r_1$ was discovered and corrected. The solutions were then integrated from t_A to t_B. There was a subsequent local adjustment of the solution near the inner wall to the resultant change in stress at r_1 in the equation for v (A 3c). The adjustment took place relatively rapidly and was mainly confined to a region near r_1. The total change was small and away from the vicinity of the inner wall the solutions appeared to continue, without noticeable distortion, the same trend towards a steady state as before t_A. At t_B, the solutions again appeared to be close to steady-state values.

In connexion with the question of obtaining an 'approximate steady-state' solution, results from investigations of the spin-up of rotating stratified fluids (Holton 1965; Pedlosky 1967; Walin 1969; Sakurai 1969; Siegmann 1971) are useful. According to these studies, rotating stratified fluids respond initially to a change in boundary conditions, such as in the problems here, on a time scale $t = O(E^{-\frac{1}{2}})$. They subsequently adjust to a steady state on a longer, diffusive time scale $t_2 = O(E^{-1})$. A rough order-of-magnitude estimate for the decay time on the t_2 scale, with $E = 5 \times 10^{-4}$, is $t_{2D} = E^{-1} = 2000$. It is however evidently *not necessary* to integrate out to times $t \sim 2000$ to find the features of the steady-state flow. Two factors are important: first, the actual numerical size of the con-

stant λ in the relation $t_{2D} = (\lambda E)^{-1}$ for the decay time and second, the relative size, on the t_2 scale, of the transient component and the steady-state solution. The latter depends, of course, on what happens on the shorter t_1 time scale. These points are illustrated in detail below for one case for which an analytical solution to the complete unsteady problem may be obtained.

We consider the linear, initial-value, spin-up problem for the boundary conditions in $S3D$. We assume that $S = O(1)$ and $E \ll 1$. For simplicity, we use the narrow-gap approximation and employ Cartesian co-ordinates as defined in part 1 (i.e., the fluid is contained in the region $0 \leqslant x \leqslant 1$, $0 \leqslant z \leqslant 1$, the velocity vector $\mathbf{q}$ has components (u, v, w) in the (x, y, z) directions, and $\partial/\partial y \equiv 0$).

The governing equations are (2.1), with the substitution of (3.1) and terms multiplied by ϵ and F neglected. The initial conditions are

$$\mathbf{q} = 0, \quad T_p = 0, \tag{5.1a, b}$$

and the boundary conditions are

$$\mathbf{q}(z = 1) = \hat{\mathbf{j}} V_T(x) = \hat{\mathbf{j}} \sum_{n=1}^{\infty} V_{Tn} \sin n\pi x, \tag{5.2a}$$

$$\mathbf{q}(x = 0, 1) = \mathbf{q}(z = 0) = 0, \tag{5.2b}$$

$$T_{pz}(z = 0, 1) = 0, \quad T_{px}(x = 0, 1) = 0. \tag{5.2c, d}$$

We first consider the $t_1 = O(E^{-\frac{1}{2}})$ time scale and define $\tau_1 = tE^{\frac{1}{2}}$. This problem is similar in form to problems treated previously (e.g., Walin 1969), and we just outline the solution. The governing equation for the lowest order pressure, $p_p = \bar{p}(\tau_1) + \ldots$, is

$$(\bar{p}_{xx} + (4/S)\,\bar{p}_{zz})_{\tau_1} = 0, \tag{5.3}$$

with initial condition

$$\bar{p}(\tau_1 = 0) = 0 \tag{5.4a}$$

and boundary conditions

$$-S^{-1}\bar{p}_{z\tau_1} = \tfrac{1}{2}(V_{Tx} - \tfrac{1}{2}\bar{p}_{xx}) \quad \text{at} \quad z = 1, \tag{5.4b}$$

$$-S^{-1}\bar{p}_{z\tau_1} = \tfrac{1}{4}\bar{p}_{xx} \quad \text{at} \quad z = 0, \tag{5.4c}$$

$$\bar{p}_{x\tau_1} = 0 \quad \text{at} \quad x = 0, 1. \tag{5.4d}$$

This problem may be solved with the use of the Laplace transform. The solution is

$$\bar{p} = -\sum_{n=1}^{\infty} \frac{V_{Tn}}{n\pi}\left[\gamma_n \sinh \gamma_n z \left(\frac{(\alpha_n - \beta_n)}{\alpha_n \beta_n} + \frac{e^{-\alpha_n \tau_1}}{\alpha_n} - \frac{e^{-\beta_n \tau_1}}{\beta_n}\right) - \cosh \gamma_n z\,(e^{-\alpha_n \tau_1} - e^{-\beta_n \tau_1})\right] \cos n\pi x, \tag{5.5}$$

where $\gamma_n = \frac{1}{2}n\pi S^{\frac{1}{2}}$, $\alpha_n = \bar{\lambda}_n + \bar{\delta}_n$, $\beta_n = \bar{\lambda}_n - \bar{\delta}_n$, $\bar{\lambda}_n = \gamma_n \coth \gamma_n$ and

$$\bar{\delta}_n = \gamma_n (\sinh \gamma_n)^{-1}.$$

For $\tau_1 \gg 1$, the solution reaches a quasi-steady state given by

$$\bar{p} \simeq -2 \sum_{n=1}^{\infty} \frac{V_{Tn}}{n\pi} \frac{\sinh \gamma_n z}{\sinh \gamma_n} \cos n\pi x. \tag{5.6}$$

The mode ($n = 1$) that decays most slowly with time has, for $S = 1{\cdot}1$, $\alpha_1 = 2{\cdot}4$ and $\beta_1 = 1{\cdot}1$. The largest decay time results from β_1 and, for $E = 5 \times 10^{-4}$, is $t_{1D} \simeq 41$. The temperature field adjusts to satisfy the boundary conditions (5.2c) at $z = 0$, 1 in diffusion layers of thickness $O(E^{\frac{1}{4}})$ (Pedlosky 1967). The correction for p in these layers is $O(E^{\frac{1}{2}})$.

We next consider the $t_2 = O(E^{-1})$ time scale and define $\tau_2 = tE$. The governing equation for the lowest order pressure, $p_p = \tilde{p}(\tau_2) + \ldots$, is (Pedlosky 1967)

$$[\tilde{p}_{xx} + (4/S)\,\tilde{p}_{zz}]_{\tau_2} = \nabla^2[\tilde{p}_{xx} + (4/\sigma S)\,\tilde{p}_{zz}], \tag{5.7}$$

where $\nabla^2 = \partial^2/\partial x^2 + \partial^2/\partial z^2$. The boundary conditions on $\tilde{p}$ from (5.2) (part 1) are

$$\tilde{p}_x(z = 1) = 2V_T, \quad \tilde{p}_{zz}(z = 1) = 0; \tag{5.8a,b}$$

$$\tilde{p}_x(z = 0) = 0, \quad \tilde{p}_{zz}(z = 0) = 0; \tag{5.8c,d}$$

$$\tilde{p}_x(x = 0, 1) = \tilde{p}_{xxx}(x = 0, 1) = 0. \tag{5.8e,f}$$

The initial condition for $\tilde{p}$ comes from matching with the solution on the τ_1 scale, i.e.

$$\tilde{p}(\tau_2 \to 0) = \overline{p}(\tau_1 \to \infty). \tag{5.9}$$

To solve for $\tilde{p}$ we define $$\tilde{p} = p_S + \tilde{p}_T, \tag{5.10}$$

where p_S is the final steady-state solution (part 1),

$$p_S = -2\sum_{n=1}^{\infty} \frac{V_{Tn}}{n\pi[1 - (4/\sigma S)]}\left(\frac{\sinh n\pi z}{\sinh n\pi} - (4/\sigma S)\frac{\sinh \frac{1}{2}n\pi(\sigma S)^{\frac{1}{2}}z}{\sinh \frac{1}{2}n\pi(\sigma S)^{\frac{1}{2}}}\right)\cos n\pi x, \tag{5.11}$$

and $\tilde{p}_T$ is a transient component. The initial condition for $\tilde{p}_T$ is

$$\tilde{p}_T(\tau_2 \to 0) = \overline{p}(\tau_1 \to \infty) - p_S. \tag{5.12}$$

The boundary conditions for $\tilde{p}_T$ are homogeneous and are given by (5.8) with (5.8a) replaced by $\tilde{p}_{Tx}(z = 1) = 0$. The solution (Pedlosky 1967) is

$$\tilde{p}_T = \sum_{m=1}^{\infty}\sum_{n=1}^{\infty} A_{mn} \sin m\pi z \cos n\pi x e^{-\lambda_{mn}\tau_2}, \tag{5.13a}$$

where $$\lambda_{mn} = \pi^2(n^2 + m^2)\,[n^2 + (4/\sigma S)\,m^2]\,[n^2 + (4/S)\,m^2]^{-1} \tag{5.13b}$$

and $$A_{mn} = 4(-1)^m V_{Tn}(m/n)\,\pi^{-2}\{(m^2 + \tfrac{1}{4}Sn^2)^{-1} - [1 - (4/\sigma S)]^{-1} \times [(m^2 + n^2)^{-1} - (4/\sigma S)\,(m^2 + \tfrac{1}{4}\sigma S n^2)^{-1}]\}.$$

For $S = 1{\cdot}1$ and $E = 5 \times 10^{-4}$, the decay time for the most slowly decaying mode ($m = 1, n = 1$) is $t_{2D} = (\lambda_{11}E)^{-1} = (6{\cdot}46E)^{-1} = 310$. Note that this is quite a bit smaller than $E^{-1} = 2000$. For a value of $t_B = 210$ we find $\exp(-\lambda_{11}Et_B) = 0{\cdot}51$, which is not that large a decay. However, the importance of $\tilde{p}_T$ in clouding the steady-state picture also depends on its magnitude relative to p_S. If we compare, for $S = 1{\cdot}1$, the initial ($\tau_2 = 0$) magnitude of the most slowly decaying transient mode ($n = 1$, $m = 1$) (5.13) with the magnitude of the $n = 1$ component of the steady-state solution (5.11), we find, for example, at $z = 0{\cdot}5$, that

$$\tilde{p}_{T11}/p_{S1}(= \tilde{v}_{T11}/v_{S1}) \simeq \tfrac{1}{4}.$$

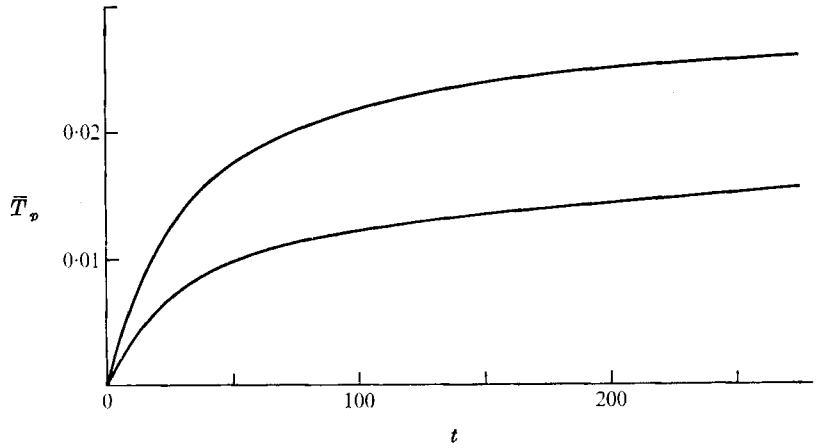

FIGURE 6. Values from solution $S3$ of $\bar{T}_p = T - z$ as a function of time from the calculation of the unsteady flow. The upper curve is for $\bar{T}_p$ ($r = 1{\cdot}49$, $z = 0{\cdot}743$); the lower curve is for $\bar{T}_p$ ($r = 1{\cdot}49, z = 0{\cdot}492$).

The transient mode $\tilde{p}_{T11}$ therefore has an initial magnitude which is generally small compared with p_{S1}. Since the higher order modes decay much more rapidly than $\tilde{p}_{T11}$, we would expect that, for moderate values of τ_2, $\tilde{p}_T$ would be small compared with p_S and that the characteristics of p_S could therefore be determined from an examination of $\tilde{p}$. Furthermore, because p_S satisfies the boundary conditions, the lower modes of $\tilde{p}_T$ will be small near the boundaries where the major part of the upwelling circulation, which is the main feature of interest, takes place. In addition, the higher modes, with more structure, which could affect the details of the upwelling circulation, decay rapidly. Assuming that the relative magnitudes of p_S and $\tilde{p}_T$ indicate the relative magnitudes of the other flow variables, we conclude that, for this problem, numerical integration times $t_B \simeq 200$ should be adequate to reveal the important features of the steady solution.

For the other boundary conditions in the numerical solutions, analytical results on the t_2 time scale are not as readily obtained. However, from an examination of the numerical solutions, we draw a similar conclusion. For the velocity-driven cases there is, at times t_B, essentially a quasi-steady balance in all of the equations except the energy equation (2.1c), as is illustrated in figures 3, 4 and 5 for $S3$. In (2.1c), the unsteady term is relatively small near the top and bottom surfaces where, in the case of the upwelling region near the top surface, it was desirable to draw some conclusions on the relative size of the nonlinear terms. In the stress-driven case $S3E$, the unsteady term in the v momentum equation is not negligible and has about the same relative size as the unsteady term in the temperature equation, as shown in figures 4 and 5 for $S3$. To give a further indication of the time variation that remains in the solutions, e.g. in $S3$, the values at two points of the difference in temperature from the initial conditions,

$$\bar{T}_p = T - z,$$

are plotted as a function of time in figure 6. It can be seen that at the end of the computation the final steady values have not been reached. However, the rate of change is decreasing and it appears that a large fraction of the total change has been accomplished. (Note that there is no noticeable change in behaviour after t_A.)

We have also checked these ideas by numerically integrating, on a coarse grid with 25×32 mesh cells, the solutions $S2$ and $S3$ out to times $t_B > 1000$. These solutions agree well (see § 6) with the original fine-grid solutions. The results showed that (i) the changes in the solutions between $t = 211$ and $t = 1037$ were relatively small and that (ii) the qualitative differences in the solutions $S2$ and $S3$ at $t = 1037$ were also shown at $t = 211$.

In summary, it is clear that there will be small quantitative changes in the original solutions, governed by diffusive processes, during the final approach to a steady state. The numerical methods that we used, however, are inefficient for the calculation of diffusion processes (see appendix) and would require the expenditure of a great deal of computer time for the calculation of perfectly steady solutions. We felt that this was not worthwhile and therefore terminated the computations at a point where we thought the important elements of the steady solutions were sufficiently resolved. We feel that the remaining changes would definitely not alter the essential features of the solutions, especially their *relative* nature, and therefore would not alter the qualitative conclusions that we have drawn.

6. Numerical resolution

With regard to the accuracy of the resolution of the solution by the finite-difference approximations, the number of mesh cells was 50 and 64 in the r and z directions. The value of the Ekman number was set so that there were approximately five cells in the Ekman layers in solution $S1$ with $S = 0$. Outside the corner regions, the largest gradients were exhibited in the Ekman layers in $S1$. To check the resolution there, a comparison of the exact solution for the linear Ekman layer and the results from the numerical solution $S1$ at time t_A was made for the boundary layer on the top surface, along the line $r = 1{\cdot}48$. The linear-theory solution

$$v = V_I - [(V_I - V_B)\cos\zeta - U_I \sin\zeta]\, e^{-\zeta}, \tag{6.1a}$$

$$u = U_I - [U_1 \cos\zeta + (V_I - V_B)\sin\zeta]\, e^{-\zeta}, \tag{6.1b}$$

where $\zeta = E^{-\frac{1}{2}}(1-z)$ and where U_I and V_I and V_B are the interior and boundary values, respectively, was calculated using the interior values from the numerical solution. The results are compared in figure 7. It can be seen that the agreement is quite good. The only substantial disagreement is in the value of u at the first grid point, half a cell length from the boundary, where the magnitude of the error is 23·9 %. As the stratification is increased the Ekman layers become weaker and the gradients smaller. It is felt that the resolution was sufficiently accurate for our purposes.

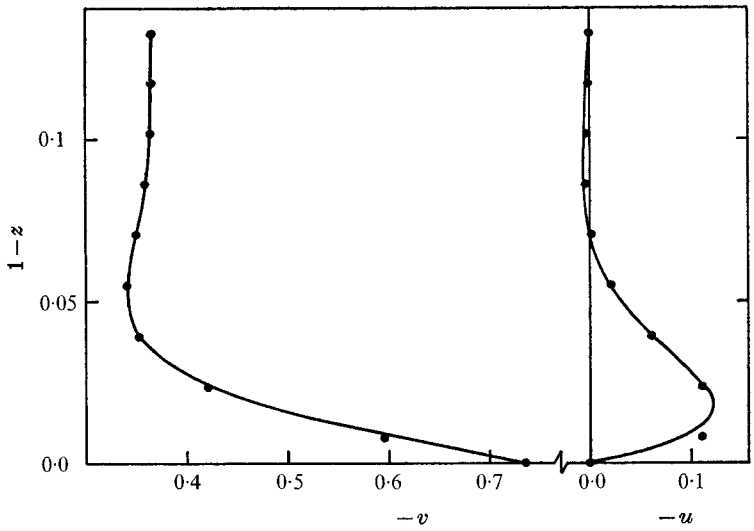

FIGURE 7. A comparison of the exact linear solution (6.1*a*, *b*) (solid lines) and the results (●) from the numerical solution *S* 1 at time t_A for the Ekman layer on the top surface at $r = 1{\cdot}47$ (for v) and $r = 1{\cdot}48$ (for u).

In most of the solutions there is a concentrated flow very close to the upwelling corner. It cannot be expected that all the details of the flow in that region are accurately resolved. However, the corner region is, according to linear theory, essentially passive. Since the difference approximations conserve mass exactly, there will be overall mass conservation in the corner region and the lack of resolution in this area should, we hope, not affect, to a significant extent, the remainder of the flow field.

It was unfortunately not practical to check the resolution of the solution by reducing the grid size. A fast Fourier transform that is restricted to a number of points that is a power of two was used in the z direction in solving the Poisson equation for the pressure. A reduction of the grid size in the z direction was therefore restricted to a doubling of the number of points in that direction. This would have resulted in a total number of grid points that was too large for the computational facilities. The calculation of solutions with a larger grid size was possible, of course, and this was done for solutions *S* 2 and *S* 3 with 25×32 mesh cells. Calculations were carried out to time $t_B = 1037$. Considering the coarseness of this grid, the agreement with the original solutions, as judged by a comparison of the contour plots, was reasonably good. The flows were qualitatively very similar. The most sensitive plot was that of ψ, where, although the pattern was similar, the exact location of the streamlines differed. The values of

$$\psi_{\max} \times 10^3 = 3{\cdot}68,\ 2{\cdot}83$$

were close to those in the original *S* 2 and *S* 3. It is felt that the good qualitative agreement of the coarse-grid solutions indicated that the original solutions have enough resolution to resolve the features about which we have drawn conclusions.

7. Summary

The axisymmetric, mechanically driven, approximately steady motion of a stratified fluid in a rotating annulus has been studied with the use of numerical solutions to finite-difference approximations. Changes in the flow field caused by variations in the stratification S, the Rossby number ϵ and the boundary conditions were investigated. Particular attention was given to a study of the changes in the meridional, or upwelling, circulation. It was found that the upwelling circulation is strongly dependent on the stratification S. For $S = 0$, the upwelling fluid comes from the bottom in a side-wall boundary layer. For larger values of S (with $\bar{S} = O(1)$), the nature of the circulation changes. Upwelling continues at the outer side wall, but the fluid is fed to the surface layer directly from the interior, with no involvement in a side-wall boundary layer. A large part of the circulation is confined to a region near the surface. As S is increased, the upwelling circulation weakens and the region it occupies shrinks towards the top surface.

Nonlinear convective effects in the energy equation are observed in the upwelling and downwelling regions at a Rossby number $\epsilon = 0{\cdot}1$. These are apparently related to the specific nature of the flow which is produced by an applied velocity with non-zero values at the side walls. Increasing the Rossby number leads to larger temperature gradients in the interior and to larger convective distortion of the isotherms in the upwelling and downwelling corners. Nonlinear effects appear to be decreased by an increase in the stratification. Also, the nonlinear effects are larger, and the meridional circulation is noticeably stronger, in regions where the local stratification is decreased by the fluid motion. This is illustrated by a comparison of upwelling and downwelling cases and by a comparison of upwelling with a fixed temperature and with a fixed heat flux boundary condition on the top surface.

The computations were made with the computer facilities of the National Center for Atmospheric Research (NCAR), which is sponsored by the National Science Foundation. The computations were initiated while the author was a scientific visitor at NCAR during the summer of 1970. The author wishes to thank Dr J. W. Deardorff, Dr D. G. Fox, Dr S. A. Orszag and Dr D. K. Lilly for helpful discussions of numerical methods and computational techniques. This research was partially supported by the Atmospheric Sciences Section, National Science Foundation, under NSF grant GA-18109, and by the Oceanography Section, National Science Foundation, under NSF grant GA-30592.

Appendix. Numerical methods

The governing equations (2.1) for axisymmetric flow in cylindrical-polar co-ordinates, with (u, v, w) as the velocity components in the (r, θ, z) directions, are

$$r^{-1}(ru)_r + w_z = 0, \tag{A 1a}$$

$$u_t + \epsilon(D(u) - r^{-1}v^2) - 2v = -p_r + EJ(u), \tag{A 1b}$$

$$v_t + \epsilon(D(v) + r^{-1}uv) + 2u = EJ(v), \tag{A 1c}$$

$$w_t + \epsilon D(w) = -p_z + (S/\epsilon)\,T + E\nabla^2 w, \tag{A 1d}$$

$$T_t + \epsilon D(T) = (E/\sigma)\,\nabla^2 T, \tag{A 1e}$$

where

$$D(\phi) = r^{-1}(ru\phi)_r + (w\phi)_z, \tag{A 2a}$$

$$J(\phi) = [r^{-1}(r\phi)_r]_r + \phi_{zz}, \quad \nabla^2\phi = r^{-1}(r\phi_r)_r + \phi_{zz}, \tag{A 2b, c}$$

and where the nonlinear convection terms have been written in conservation form with the use of (2.1*a*).

Finite-difference approximations to (A 1) are solved for an initial-value problem. The finite-difference methods that we have used are those which Williams (1969, 1971) has employed effectively for the calculation of unsteady three-dimensional flows. The r, z plane is divided into uniform rectangular cells with sides of length Δr and Δz which are parallel, respectively, to the r and z axes. The centres of the cells form a grid at which p, T and v are defined. The velocity components u and w are defined at points on the cell boundaries such that the u points are centred on the vertical (r = constant) boundaries and the w points are centred on the horizontal (z = constant) boundaries. These points then form a staggered grid system. Boundary surfaces of the annulus are placed along the cell boundaries. The grid extends half a cell length beyond the physical boundaries. Values of the variables at these external points are defined by the boundary conditions (A 4) and (A 5). The time variable is also divided into increments of size Δt such that $t = n\Delta t$, where n is an integer. We use the notation

$$\phi(t) = \phi(n\Delta t) = \phi^n,$$

where ϕ represents any dependent variable.

The difference equations can be written in a compact form, as in Williams (1969), if the following difference and averaging operators are defined:

$$\delta_x\phi = [\phi(x + \tfrac{1}{2}\Delta x) - \phi(x - \tfrac{1}{2}\Delta x)]/\Delta x, \quad \delta_{xx}\phi = \delta_x\delta_x\phi,$$

$$\overline{\phi}^x = \tfrac{1}{2}[\phi(x + \tfrac{1}{2}\Delta x) + \phi(x - \tfrac{1}{2}\Delta x)],$$

where x represents any independent variable.

The difference approximations to (A 1) are

$$r^{-1}\delta_r(ru) + \delta_z w = 0, \tag{A 3a}$$

$$\delta_t\overline{u}^t + \epsilon[r^{-1}\delta_r(\overline{ru}^r\overline{u}^r) + \delta_z(\overline{w}^r\overline{u}^z) - \overline{(v^2r^{-1})}^r] - 2\overline{v}^r = -\delta_r p + E\{\delta_r[r^{-1}\delta_r(ru)] + \delta_{zz}u\}_{\text{lag}}, \tag{A 3b}$$

$$\delta_t\overline{v}^t + \epsilon[r^{-1}\delta_r(ru\overline{v}^r) + \delta_z(w\overline{v}^z) + r^{-2}v(\overline{ru})^r] + 2r^{-1}(\overline{ru})^r = E\{\delta_r[r^{-1}\delta_r(rv)] + \delta_{zz}v\}_{\text{lag}}, \tag{A 3c}$$

$$\delta_t\overline{w}^t + \epsilon[r^{-1}\delta_r(\overline{ru}^z\overline{w}^r) + \delta_z(\overline{w}^z\overline{w}^z)] = -\delta_z p + (S/\epsilon)\,\overline{T}^z + E[r^{-1}\delta_r(r\delta_r w) + \delta_{zz}w]_{\text{lag}}, \tag{A 3d}$$

$$\delta_t\overline{T}^t + \epsilon[r^{-1}\delta_r(ru\overline{T}^r) + \delta_z(w\overline{T}^z)] = (E/\sigma)\,[r^{-1}\delta_r(r\delta_r T) + \delta_{zz}T]_{\text{lag}}. \tag{A 3e}$$

If the time difference is centred on the level n, then the other terms in (A 3), with the exception of the viscous and heat conduction terms, are evaluated at level n. The diffusive terms are evaluated at the level $n-1$ and are designated by a subscript 'lag'.

The boundary conditions (2.2), in difference form, are

$$w = \bar{u}^z = \bar{v}^z = 0, \quad \bar{T}^z = 0 \quad \text{at} \quad z = 0; \tag{A 4a}$$

$$w = \bar{u}^z = 0, \quad \bar{v}^z = -\tfrac{1}{2}r, \quad \bar{T}^z = 1 \quad \text{at} \quad z = 1; \tag{A 4b}$$

$$u = \bar{w}^r = \bar{v}^r = 0, \quad \delta_r T = 0 \quad \text{at} \quad r = 1, 2. \tag{A 4c}$$

The conditions (2.3a–d) become, respectively,

$$\bar{v}^z(z = 1) = \tfrac{1}{2}r, \tag{A 5a}$$

$$\delta_z T(z = 1) = \delta_z T(z = 0) = 1, \tag{A 5b}$$

$$\delta_z v(z = 1) = C_1 + C_2(r - 1), \tag{A 5c}$$

$$\bar{T}^r(r = 1) = \bar{T}^r(r = 2) = z. \tag{A 5d}$$

If we assume that the variables are known at time levels less than $n+1$, then u, v, w and T at level $n+1$ may be obtained from (A 3b–e). The pressure at $n+1$ is obtained from the solution to a Poisson equation, as described by Williams (1969), which is derived from the requirement that the continuity equation (A 3a) be satisfied at level $n+2$. To derive that equation we write (A 3b, d) in the shorthand form

$$(u^{n+2} - u^n)/2\Delta t = -\delta_r p^{n+1} + GU^{n+1,n}, \tag{A 6a}$$

$$(w^{n+2} - w^n)/2\Delta t = -\delta_z p^{n+1} + GW^{n+1,n}, \tag{A 6b}$$

where GU and GW represent the remaining terms. If the continuity equation (A 3a) at level $n+2$ is formed using the velocity components defined by (A 6a, b), we find that

$$\begin{aligned} 0 = r^{-1}\delta_r(ru^{n+2}) + \delta_z w^{n+2} = (r^{-1}\delta_r(ru^n) + \delta_z w^n) - 2\Delta t\,[r^{-1}\delta_r(r\delta_r p^{n+1}) \\ + \delta_{zz} p^{n+1} - r^{-1}\delta_r(rGU^{n+1,n}) - \delta_z GW^{n+1,n}], \end{aligned} \tag{A 7}$$

or

$$\begin{aligned} r^{-1}\delta_r(r\delta_r p^{n+1}) + \delta_{zz} p^{n+1} = [r^{-1}\delta_r(ru^n) + \delta_z w^n]/2\Delta t \\ + r^{-1}\delta_r(rGU^{n+1,n}) + \delta_z GW^{n+1,n}. \end{aligned} \tag{A 8}$$

The pressure at $n+1$ is obtained by solving the Poisson equation (A 8). The continuity equation (A 3a) at level n is left on the right-hand side to correct for the effect of any error in its solution at level n.

It is worthwhile to point out a simplification in the application of boundary conditions to (A 8). On all the boundaries, in this problem, the normal component of velocity vanishes. A direct application of this condition to the velocity component in the continuity equation (A 7), for a mesh cell next to the boundary, results immediately in an application of the proper condition to the Poisson

equation (A 8) for the pressure.† For example, the continuity equation for a cell centred at (r_0, z_0) is

$$r^{-1}\delta_r(ru) + [w(z_0 + \tfrac{1}{2}\Delta z) - w(z_0 - \tfrac{1}{2}\Delta z)]/\Delta z = 0.$$

If, however, there is a boundary along the line $z = z_0 - \frac{1}{2}\Delta z$, then $w(z_0 - \frac{1}{2}\Delta z) \equiv 0$ and the difference equation (A 6*b*) for $w(z_0 - \frac{1}{2}\Delta z)$ does not have to be written. For this cell, (A 7) becomes

$$\begin{aligned} 0 &= r^{-1}\delta_r(ru^{n+2}) + w^{n+2}(z_0 + \tfrac{1}{2}\Delta z)/\Delta z \\ &= r^{-1}\delta_r(ru^n) + w^n(z_0 + \tfrac{1}{2}\Delta z)/\Delta z - 2\Delta t[r^{-1}\delta_r(r\delta_r p^{n+1}) \\ &\quad + \delta_z p^{n+1}(z_0 + \tfrac{1}{2}\Delta z)/\Delta z - r^{-1}\delta_r(rGU^{n+1,n}) - GW^{n+1,n}(z_0 + \tfrac{1}{2}\Delta z)/\Delta z]. \quad \text{(A 9)} \end{aligned}$$

The values of p, u, w, GU and GW involved in (A 9) are all defined at points inside the boundary. When this procedure is followed for all the boundary cells, the resulting set of difference equations for the pressure involves only values of the above variables at interior points and is ready for solution. Boundary conditions for the pressure do not have to be considered, since the proper boundary condition has already been applied through the vanishing of the normal component of velocity. Iterative or direct methods can be used immediately to solve the resulting equations.

An additional advantage of not using an equation for the normal component of velocity on the boundary is that the viscous terms can be written as they are in (A 3) and the equations still only require variables defined at external grid points a distance of half a mesh length outside the boundary. Although Williams (1969) defines the viscous terms through the vorticity (i.e. $-E\nabla \times \nabla \times \mathbf{q}$), which results in (A 3*b*) in the replacement of $\delta_r[r^{-1}\delta_r(ru)]$ by $-\delta_{rz}w$ and in (A 3*d*) in the replacement of $\delta_{zz}w$ by $-r^{-1}\delta_r(r\delta_z u)$, this is not absolutely necessary. While the contribution to the forcing term in the Poisson equation (A 8), from the difference approximation of the viscous terms using the vorticity, vanishes identically, as does the differential expression, the contribution from the formulation in (A 3*b*, *d*) will also vanish if (A 3*a*) at level n is satisfied. Since the error in the solution to (A 3*a*), when direct methods are used to solve (A 8), is limited to round-off error and is therefore usually very small, there appear to be no disadvantages in the use of (A 3*b*, *d*). A possible advantage of the formulation in (A 3*b*, *d*), where the viscous terms involve the same variable as the time derivative, is that if a different method for treating the time differencing of the viscous terms, e.g. an implicit method, is sought, the spatial differencing in (A 3*b*, *d*) might prove more convenient.

To solve (A 8) we used a direct method similar to that described by Williams (1969). The variables were expanded in a cosine series in the z direction. If the boundary conditions for (A 8) are applied as we have discussed, the pressure and the forcing function can be expanded immediately, without further manipulation, in the cosine series given by Williams (1969). This is because the finite cosine series expansion for p, which satisfies the difference equations (A 8) in the interior (i.e. results in a separation of variables), also satisfies the difference equations,

† This fact was used by Harlow & Welch (1965) in deriving boundary conditions for the pressure, but their procedure was different.

e.g. (A 9), at the boundary cells. A fast Fourier transform routine from the Library of the Computing Facility of the National Center for Atmospheric Research was used to expand and to invert the variables in the cosine series. Gaussian elimination was used in the r direction, with proper consideration given to the solution for the degenerate mode.

It was felt that a better estimate of the stability condition for (A 3) should be obtained. For that purpose, the following linearized set of difference equations in Cartesian co-ordinates is considered:

$$\delta_x u + \delta_z w = 0, \tag{A 10a}$$

$$\delta_t \bar{u}^t + \epsilon D_d(u) - 2\bar{v}^x = -\delta_x p + E\nabla_d^2 u_{\text{lag}}, \tag{A 10b}$$

$$\delta_t \bar{v}^t + \epsilon D_d(v) + 2\bar{u}^x = E\nabla_d^2 v_{\text{lag}}, \tag{A 10c}$$

$$\delta_t \bar{w}^t + \epsilon D_d(w) = -\delta_z p + \bar{T}_p^z + E\nabla_d^2 w_{\text{lag}}, \tag{A 10d}$$

$$\delta_t \bar{T}_p^t + \epsilon D_d(T_p) + S\bar{w}^z = (E/\sigma)\nabla_d^2 T_{p\text{lag}}, \tag{A 10e}$$

where $$D_d(\phi) = U_0 \delta_x \bar{\phi}^x + W_0 \delta_z \bar{\phi}^z, \quad \nabla_d^2 \phi = \delta_{xx}\phi + \delta_{zz}\phi,$$

and where U_0 and W_0 are constants.

We attempt to obtain a von Neumann necessary condition (Richtmyer & Morton 1967, §4.7) for the stability of (A 10) by examining the behaviour of a typical Fourier component. We therefore let

$$u = u_0 \xi^n f, \quad v = v_0 \xi^n f, \quad w = w_0 \xi^n f, \tag{A 11}$$

$$T_p = T_{p0} \xi^n f, \quad p = p_0 \xi^n f,$$

where $$f = \exp\{i[(\alpha/\Delta x)x + (\beta/\Delta z)z]\}, \quad 0 \leqslant \alpha \leqslant 2\pi, \quad 0 \leqslant \beta \leqslant 2\pi,$$

and where u_0, v_0, w_0, T_{p0} and p_0 are constant coefficients and ξ is an amplification factor.

The substitution of (A 11) in (A 10) results in a set of five homogeneous linear equations for the five coefficients. In order for there to be non-trivial solutions, the determinant of the coefficients must vanish. This results in an algebraic equation for ξ. For stability, it is required that $|\xi| \leqslant 1$ and this gives conditions on the time step. These conditions can be found easily if it is assumed that the Prandtl number $\sigma = 1$. In that case, the equation for ξ reduces to

$$\xi^2 - 2\Delta t i(-F \pm G)\xi - (1 + 2\Delta t H) = 0, \tag{A 12}$$

where $$F = \epsilon(U_0 q \sin\alpha + W_0 s \sin\beta), \tag{A 13a}$$

$$G = \left\{\frac{4s^2\cos^2(\tfrac{1}{2}\alpha)\sin^2(\tfrac{1}{2}\beta) + Sq^2\cos^2(\tfrac{1}{2}\beta)\sin^2(\tfrac{1}{2}\alpha)}{q^2\sin^2(\tfrac{1}{2}\alpha) + s^2\sin^2(\tfrac{1}{2}\beta)}\right\}^{\frac{1}{2}}, \tag{A 13b}$$

$$H = 2E[q^2(\cos\alpha - 1) + s^2(\cos\beta - 1)] \tag{A 13c}$$

and $$q = 1/\Delta x, \quad s = 1/\Delta z.$$

In order for the solution of (A 12) to have $|\xi| \leqslant 1$, the coefficients must satisfy the inequalities

$$|1 + 2\Delta t H| \leqslant 1 \tag{A 14a}$$

and $$2\Delta t|-F \pm G| \leqslant |2 + 2\Delta t H|. \tag{A 14b}$$

From (A 14a) we find that

$$\Delta t \leqslant [4E(q^2+s^2)]^{-1}. \tag{A 15}$$

With the use of (A 15) we obtain, from (A 14b),

$$\Delta t \leqslant \min_{0\leqslant\alpha\leqslant 2\pi,\ 0\leqslant\beta\leqslant 2\pi} (F+G+H)^{-1}. \tag{A 16}$$

A sufficient condition for the satisfaction of (A 16) is

$$\Delta t \leqslant [\epsilon(qU_0+sW_0)+\max(2, S^{\frac{1}{2}})+4E(q^2+s^2)]^{-1}, \tag{A 17}$$

which implies (A 15). Recall that we assumed $\sigma = 1$. It appears from (A 15) that the condition for $\sigma \geqslant 1$ should be satisfied if (A 17) is satisfied. Because of the approximations, this condition should naturally be used only as a guide, with local values of u and w replacing U_0 and W_0.

In our problem, by far the most restrictive contribution to the limit on the time step in (A 17) is from the diffusion terms. The next most restrictive contribution, in this relatively low Rossby number axisymmetric flow, is from the condition $\max(2, S^{\frac{1}{2}})$ from the inertial–internal waves. In the calculations (performed before the derivation of (A 17)) we used $\Delta t = C_0(8Es^2)^{-1} \simeq 0{\cdot}061C_0$, where $C_0 = 0{\cdot}7$–$0{\cdot}8$. Because of the factor C_0 and because $\Delta r = 1{\cdot}28\Delta z$, this value of Δt was usually smaller than that given by (A 17). To prevent the 'time splitting' instability (Williams 1969) the variables at levels $n+1$ and n, and at n and $n-1$, were averaged, and the time dropped back $\frac{1}{2}\Delta t$ every 30 time steps. On the CDC 6600, 1·63 s were required to calculate one time-step, with 55 % of that time used for the solution of the Poisson equation.

It has been pointed out that the size of the time step is limited essentially by the contribution to the stability condition arising from the viscous and heat diffusion terms. Without this contribution, Δt could have been increased typically, in this problem, by a factor of about 5. It seems therefore that a more efficient method of treating the time differencing of the viscous terms should be developed for use with the other desirable features of the scheme. The present method of lagging these terms suffers on three counts.

(i) If we assume, for simplicity, that the grid spacing is equal in both directions and if we consider only the major contribution to (A 17), we have $\Delta t \leqslant \Delta z^2/8E$. Although the time step is limited by the square of the spatial grid increment, the usual argument is that, if the Ekman number E is very small, this condition is not restrictive. However, in the annulus problem there are Ekman layers, which have a dimensionless thickness $\delta \simeq 2E^{\frac{1}{2}}$ on the horizontal surfaces. The number of grid points in an Ekman layer is approximately $N_B \simeq 2E^{\frac{1}{2}}/\Delta z$. It follows that $\Delta z \simeq 2E^{\frac{1}{2}}/N_B$ and that therefore $\Delta t \leqslant \frac{1}{2}N_B^{-2}$. This relation shows that the time step is essentially limited by the inverse square of the number of points in the boundary layers, regardless of the value of E. For a reasonable number of points in the Ekman layers, this condition turns out to be very restrictive. It becomes more restrictive if additional resolution is desired in these layers.

(ii) The truncation error, due to the time differencing of the diffusion terms, is of the order of the time step Δt. A more accurate scheme with an error of order

Δt^2 (which is the truncation error from the time differencing of the rest of the terms in the equations) would be desirable.

(iii) The final approach to a steady solution in rotating stratified fluids is governed by diffusion processes and, as a result, the total number of time steps required to reach a steady state is excessive. The dimensionless time scales for diffusion processes in (A 1) are $t_d \simeq E^{-1}$ and σE^{-1}. The total number of time steps required to reach a steady state is therefore approximately $t_d/\Delta t = 8\sigma/\Delta z^2$ (for $\sigma > 1$). A similar estimate holds for the attainment of a steady solution of the simple heat diffusion equation when the same type of difference scheme is used. The explicit method is well known to be inefficient in that case and it is just as inefficient for the Navier–Stokes equations.

Perhaps fractional-steps methods (Richtmyer & Morton 1967, § 8.9) could be used for the diffusion terms and incorporated successfully with the other desirable features of the scheme in (A 3). This matter, however, requires further study.

REFERENCES

Allen, J. S. 1972 Upwelling of a stratified fluid in a rotating annulus: steady state. Part 1. Linear theory. *J. Fluid Mech.* **56**, 429–445.

Barcilon, V. 1970 Some inertial modifications of the linear viscous theory of steady rotating fluid flows. *Phys. Fluids*, **13**, 537–544.

Barcilon, V. & Pedlosky, J. 1967*a* Linear theory of rotating stratified fluid motions. *J. Fluid Mech.* **29**, 1–16.

Barcilon, V. & Pedlosky, J. 1967*b* A unified linear theory of homogeneous and stratified rotating fluids. *J. Fluid Mech.* **29**, 609–621.

Greenspan, H. P. 1968 *The Theory of Rotating Fluids.* Cambridge University Press.

Harlow, F. H. & Welch, J. E. 1965 Numerical calculation of time-dependent viscous incompressible flow of fluid with free surface. *Phys. Fluids*, **8**, 2182–2189.

Holton, J. R. 1965 The influence of viscous boundary layers on transient motions in a stratified fluid, part I. *J. Atmos. Sci.* **22**, 402–411.

Pedlosky, J. 1967 The spin up of a stratified fluid. *J. Fluid Mech.* **28**, 463–479.

Pedlosky, J. 1970 *Notes on the* 1970 *Summer Program in Geophysical Fluid Dynamics*, The Woods Hole Oceanographic Institution, no. 70–50, vol. **1**, 1–67.

Richtmyer, R. D. & Morton, K. W. 1967 *Difference Methods for Initial-Value Problems.* Interscience.

Sakurai, T. 1969 Spin-down problem of rotating stratified fluid in thermally insulated circular containers. *J. Fluid Mech.* **37**, 689–699.

Siegmann, W. L. 1971 The spin down of rotating stratified fluids. *J. Fluid Mech.* **47**, 689–711.

Walin, G. 1969 Some aspects of time-dependent motion of a stratified rotating fluid. *J. Fluid Mech.* **36**, 289–307.

Williams, G. P. 1969 Numerical integration of the three-dimensional Navier–Stokes equations for incompressible flow. *J. Fluid Mech.* **37**, 727–750.

Williams, G. P. 1971 Baroclinic annulus waves. *J. Fluid Mech.* **49**, 417–449.